Abstracta

Ano XXIX - N. 05

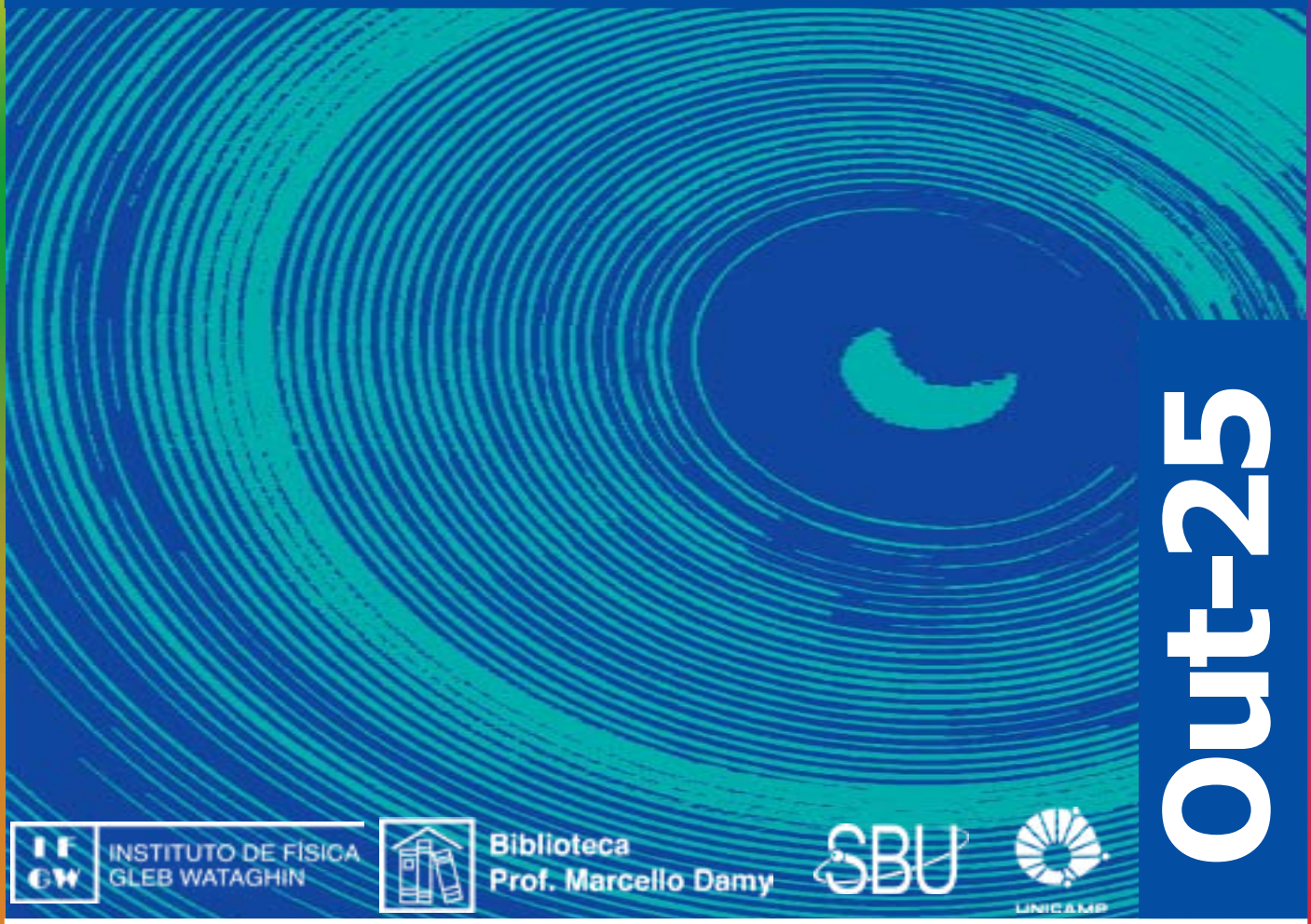

Artigos publicados - P243-2025 à P303-2025

Correções - Co003-2025 à Co005-2025

Cartas - Ca001-2025 à Ca002-2025

Conjunto de Dados - D001-2025

Defesas de Dissertações do IFGW - D016-2025 à D018-2025

Defesas de Teses do IFGW - T012-2025 à T018-2025

Novidade: **agora os trabalhos possuem os links para o texto publicado nas revistas.**

Artigos publicados

[P243-2025] "3D Carbon Nanostructures Derived from 2D Irida-Graphene: Insights into Structural, Mechanical, Electronic, and Optical Properties"

Felix, I. M.; **Oliveira, R. B. de***; Ribeiro Jr., L. A.; **Galvao, D. S.***; Pereira Jr., M. L.; Tromer, R. M.

The exploration of three-dimensional (3D) carbon allotropes has received increasing attention due to their potential in advanced materials and nanotechnology. Irida-Graphene (IG), a two-dimensional carbon allotrope with a structure consisting of 3-6-8 carbon rings, can be used as a precursor for creating 3D materials with tailored properties. This work presents a comprehensive computational characterization of four novel 3D structures derived from IG, named 3D-IG-alpha, -beta, -gamma, and -delta. These structures were generated through biaxial strain and layer compression, followed by detailed analyses of their structural, electronic, mechanical, and optical properties. Stability was confirmed via density functional theory optimizations and ab initio molecular dynamics simulations at 800 K, demonstrating structural integrity under high-temperature conditions. Electronic analyses revealed indirect band gaps ranging from 0.62 to 1.68 eV, indicating semiconducting behavior. Mechanical analyses revealed anisotropic Young's modulus values. Optical properties exhibit strong absorption and reflectivity in the ultraviolet range, making them potential candidates for UV-blocking materials.

ACS OMEGA 10[34], p. 38985-38994, 2025. DOI: 10.1021/acsomega.5c05013. **Acesso: https://doi.org/10.1021/acsomega.5c05013**

[P244-2025] "Angular analysis of the B0 --> K*(892)0μ+μ- decay in proton-proton collisions at √s=13 TeV"

Hayrapetyan, A.; Tumasyan, A.; **Chinellato, J. A.***; et al.
CMS Collaboration

A full set of optimized observables is measured in an angular analysis of the decay B-0 -> K*(892)(0)mu(+)mu(-) using a sample of proton-proton collisions at root s = 13 TeV, collected with the CMS detector at the LHC, corresponding to an integrated luminosity of 140 fb(-1). The analysis is performed in six bins of the squared invariant mass of the dimuon system, q(2), over the range 1.1 < q(2) < 16 GeV2. The results are among the most precise experimental measurements of the angular observables for this decay and are compared to a variety of predictions based on the standard model. Some of these predictions exhibit tension with the measurements.

PHYSICS LETTERS B 864, 139406, 2025. DOI: 10.1016/j.physletb.2025.139406. **Acesso: https://doi.org/10.1016/j.physletb.2025.139406**

[P245-2025] "Athos-Graphene: Computational discovery of an art-inspired 2D carbon anode for lithium-ion batteries"

Lima, K. A. L.*; Laranjeira, J. A. S.; Martins, N. F.; Sambrano, J. R.; Dias, A. C.; **Galvao, D. S.***; Ribeiro Junior, L A.

Two-dimensional (2D) carbon allotropes have attracted growing interest for their structural versatility and potential in energy storage and nanoelectronics. We propose Athos--Graphene (AG), a novel 2D carbon allotrope inspired by the geometric patterns of Brazilian artist Athos Bulc ão. Designed using density functional theory, AG features a periodic structure with high thermodynamic and thermal stability, as evidenced by a low cohesive energy (-7.96 eV/atom), the absence of imaginary phonon modes, and robust performance in ab initio molecular dynamics simulations up to 1000 K. It exhibits anisotropic mechanical properties, with maximum Young's modulus of 328.38 N/m, and Poisson's ratio ranging from 0.06 up to 0.50, respectively. Electronic structure analyses confirm its metallic behavior, while optical studies reveal anisotropic absorption in the visible and UV regions. For lithium-ion storage, AG shows strong Li adsorption (-2.3 eV to-1.0 eV), a high theoretical capacity of 836.78 mAh/g, and a low average open-circuit voltage of 0.54 V. Lithium diffusion barriers are as low as 0.30 eV on the surface and 0.66 eV between layers, with a diffusion coefficient of approximately 10-6 cm2/s. These features highlight AG as a promising anode material for high-performance lithium-ion batteries.

JOURNAL OF ENERGY STORAGE 133, 117868, 2025. DOI: 10.1016/j.est.2025.117868. **Acesso: https://doi.org/10.1016/j.est.2025.117868**

[P246-2025] "Bottom quark energy loss and hadronization with B+ and Bs0 nuclear modification factors using pp and PbPb collisions at √sNN=5.02 TeV"

Hayrapetyan, A.; Tumasyan, A.; **Chinellato, J. A.***; et al.
CMS Collaboration

The production cross sections of B-s(0) and B+ mesons are reported in proton-proton (pp) collisions recorded by the CMS experiment at the CERN LHC with a center-of-mass energy of 5.02 TeV. The data sample corresponds to an integrated luminosity of 302 pb(-1). The cross sections are based on measurements of the B-s(0)-> J/psi(mu(+)mu(-))phi(1020)(K+K-) and B+-> J/psi(mu(+)mu(-))K+ decay channels. Results are presented in the transverse momentum (p(T)) range 7-50 GeV/c and the rapidity interval |y| < 2.4 for the B mesons. The measured p(T)-differential cross sections of B+ and B-s(0) in pp collisions are well described by fixed-order plus next-to-leading logarithm perturbative quantum chromodynamics calculations. Using previous PbPb collision measurements at the same nucleon-nucleon center-of-mass energy, the nuclear modification factors, R-AA, of the B mesons are determined. For p(T)> 10 GeV/c, both mesons are found to be suppressed in PbPb collisions (with R-AA values significantly below unity), with less suppression observed for the Bs0 mesons. In this p(T) range, the R-AA values for the B+ mesons are consistent with those for inclusive charged hadrons and D-0 mesons. Below 10 GeV/c, both B+ and B-s(0) are found to be less suppressed than either inclusive charged hadrons or D-0 mesons, with the B-s(0) R-AA value consistent with unity. The R-AA values found for the B+ and B-s(0) are compared to theoretical calculations, providing constraints on the mechanism of bottom quark energy loss and hadronization in the quark-gluon plasma, the hot and dense matter created in ultrarelativistic heavy ion collisions.

JOURNAL OF HIGH ENERGY PHYSICS [2], 195, 2025. DOI: 10.1007/JHEP02(2025)195. **Acesso: https://doi.org/10.1007/JHEP02(2025)195**

[P247-2025] "Causality of polarizable dissipative fluids from Lagrangian hydrodynamics"

Montenegro, D.; **Torrieri, G.***

We perform a causality analysis on the dispersion relation of hydrodynamics with spin as well as shear and bulk viscosity, including the relaxation times for all these quantities. We find that the interplay of the three relaxational scales, for shear and bulk viscosity as well as polarization, leads to nontrivial effects on the dispersion relation.

Unexpectedly, the presence of polarization leads to lower effective viscosity and a longer relaxation time, and the presence of viscosity leads to lower limits as well as upper ones on the group velocity and constraints relating polarization to viscosity relaxation times. We conclude with a qualitative discussion on how these results impact phenomenology, specifically the low effective viscosity in strongly interacting matter as well as shear-vorticity coupling.

PHYSICAL REVIEW D 112[3], 034041, 2025. DOI: 10.1103/yjtd-qztf. **Acesso: https://doi.org/10.1103/yjtd-qztf**

[P248-2025] "Chiral and flavor oscillations in the interaction picture"

Blasone, M.; Giacosa, F.; Smaldone, L.; **Torrieri, G.***

We provide a concise review of how chiral and flavor oscillations can be described in quantum field theory using a finite--time interaction picture approach, where the mass and mixing terms in the Lagrangian can be treated as perturbations. We derive the oscillation formulas for both chiral and flavor transitions and demonstrate that, within the adopted approximations, they match the exact results obtained through non--perturbative methods. Finally, we point out the strong similarities and the differences between these two phenomena.

Journal of Physics: Conference Series 3017, 012027, 2025. DOI: 10.1088/1742-6596/3017/1/012027**. Acesso: https://iopscience.iop.org/article/10.1088/1742-6596/3017/1/012027**

[P249-2025] "Controlled synthesis and magnetic properties of BiFeO3 nanoparticles using sucrose"

Santos, B. J.; Duque, J. G. S.; Meneses, C. T.; Cunha, G. S.; Fernandes, L. A.; Silva, R. A. G.; Bittar, E. M.; Fabrelli, H.; Carvalho, M. H.; **Caffer, A. M.*; Pagliuso, P. G.*;** Mesquita, F.

BiFeO3 nanoparticles are synthesized via the co-precipitation method using sucrose as an agent to control particle size. The synthesis predominantly results in single-phase BiFeO3 with rhombohedral symmetry (space group), leading to a reduction in particle size from 50 to 25 nm with increasing sucrose concentration. Thermal analysis, performed via thermogravimetric analysis and differential scanning calorimetry, confirms the formation of a stable phase and provides insights into the crystallization dynamics. Magnetization measurements indicate superparamagnetic behavior dependent on particle size, while M & ouml;ssbauer spectroscopy confirms high purity and minimal secondary phases. The observed magnetization values are lower than theoretically predicted, suggesting that the magnetic moments of Fe3+ ions may be canted due to the Dzyaloshinskii-Moriya interaction.

PHYSICS LETTERS A 562, 131005, 2025. DOI: 10.1016/j.physleta.2025.131005. **Acesso: https://doi.org/10.1016/j.physleta.2025.131005**

[P250-2025] "Controlling Magnetic-Field-Induced Shape Memory Response in Polycrystalline Off-Stoichiometry Fe47--xMn24+xGa29 Microwires"

Vidyasagar, R.; Varga, M.; Diko, P.; Ryba, T.; **Ribeiro, P. R. T.*;** Machado, F. L. de A.; Ingvarsson, S. T.; Varga, R.

The ferromagnetic shape memory (FSM) behavior of glass--coated Fe47-xMn24+xGa29 (x = 0-8 at. %) microwires has been investigated through temperature-dependent magnetization and ac magnetic susceptibility measurements. Magnetization measurements as a function of temperature reveal an abrupt increase and decrease in magnetization upon cooling and heating, respectively, indicating characteristic thermal hysteresis (Delta T-hys) behavior typically associated with a magnetic-field-induced "diffusionless" martensitic transformation. The magnitude and width of Delta T-hys are strongly correlated with the Fe/Mn atomic ratio; notably, the Fe45Mn26Ga29 microwire exhibits a very large Delta T-hys width of 98 K, which is attributed to local deformation involving the motion of Fe and Mn atoms. Furthermore, an antiferromagnetic transition is observed in a low-temperature region, shifting from 22 to 41 K depending on composition. This shift is attributed to variations in local exchange interactions arising from unequal occupation of Fe and Mn 3d orbitals. These findings highlight a compositionally driven design strategy that enables precise tuning of FSM behavior, making Fe-Mn-Ga microwires promising candidates for use in tunable magnetic actuation and sensing technologies.

ACS MATERIALS AU, 2025. DOI: 10.1021/acsmaterialsau.5c00113 Early Access Date: AUG 2025**. Acesso: https://doi.org/10.1021/acsmaterialsau.5c00113**

[P251-2025] "Deep-inelastic scattering at TeV energies with LHC muons"

Francener, R.*; Gonçalves, V. P.; Kling, F.; Krack, P.; Rojo, J.

The LHC far-forward experiments FASER and SND@LHC have pioneered the detection of TeV-energy neutrinos produced in hard-scattering proton-proton collisions at the LHC. In addition to neutrinos, an intense flux of TeV-energy muons reaches these detectors, representing a dominant background for both neutrino studies and beyond the Standard Model searches. Here we demonstrate that this forward muon flux enables a comprehensive neutral-current deep-inelastic scattering (DIS) program at FASER with a strong kinematical overlap with the Electron Ion Collider. For the Run 3 luminosity of Lpp = 250 fb−1, more than 105 inclusive muon DIS events, of which up to 104 from charm production, are expected at FASERv. As a representative application, we demonstrate the sensitivity of muon DIS at FASERv to probe the (intrinsic) charm content of the proton at large-x. We also provide predictions for event yields of muon DIS for future FASER runs and for the proposed Forward Physics Facility.

EUROPEAN PHYSICAL JOURNAL C 85[10], 1098, 2025. DOI: 10.1140/epjc/s10052-025-14829-z. **Acesso: https://doi.org/10.48550/arXiv.2506.13889**

[P252-2025] "Distinguishing Stressor, Stress, and State Anxiety: Semantic and Physiological Insights With Machine Learning Approaches"

Lindino, M. C.; **Bortoletto, L. F.*; Lima, B. S. de*;** Soriano--Vargas, A.; **Mesquita, R. C.*;** Rocha, A.

Stress and state anxiety are natural defense mechanisms of the human body, aiding in adaptation to various scenarios and playing a crucial role in human survival. According to the diagnostic and statistical manual of mental disorders, fifth edition (DSM-5), untreated stress and state anxiety can evolve into pathological conditions such as posttraumatic stress disorder (PTSD), generalized anxiety disorder, and depression. Diagnosing these conditions typically involves professional interviews, which can be challenging due to the overlap of symptoms with other conditions, the periodic nature of these assessments, and the lack of continuous mental health monitoring. Thus, developing objective metrics for early identification and constant monitoring of stress and state anxiety is essential to prevent health deterioration and improve treatment outcomes. This work aims to establish a robust methodology for analyzing and classifying stressors, stress, and state anxiety using machine learning models.

It identifies each condition's semantic differences and physiological impacts through signals such as heart rate (HR), galvanic skin response, and blood volume pressure. It also introduces two convolutional network architectures: the single--input model, which evaluates the individual contribution of each signal, and the multi-input model, designed for inputs from multiple sensors with different sampling frequencies. Additionally, it proposes a new validation setup called repeated leave-one-subject-out cross-validation (Repeated LOSOCV) to yield more precise results by considering intra- and interindividual biological variations with small datasets.

IEEE SENSORS JOURNAL 25[17], 2025. DOI: 10.1109/JSEN.2025.3591761. **Acesso: https://ieeexplore.ieee.org/document/11098602**

[P253-2025] "Electronic and optical properties of the recently synthesized 2D Vivianites (Vivianenes): Insights from first--principles calculations"

Oliveira, R. B. de*; Ipaves, B.*; Fabris, G. da S. L.*; Slathia, S.; Pereira Jr., M. L.; Tromer, R. M.; Tiwary, C. S.; **Galvao, D. S.***

Vivianite (Fe3(PO4)2 & sdot;8H2O) is a naturally occurring layered material. In this work, we have investigated its 2D monolayer form, Vivianene, through DFT and ab initio molecular dynamics simulations. Vivianene retains the main structural features of the bulk structure and shows thermal stability at room temperature. It presents an indirect bandgap of 3.03 eV, slightly lower than bulk Vivianite (3.21 eV), with Fe d orbitals dominating the electronic states. Optical results reveal a higher optical bandgap (3.6 eV) and strong absorption in the ultraviolet region. The refractive index and reflectivity indicate efficient light absorption. These results pose Vivianene as a promising 2D material for optoelectronics, sensing, and energy-related technologies applications.

SOLID STATE COMMUNICATIONS 404,116101, 2025. DOI: 10.1016/j.ssc.2025.116101. **Acesso: https://doi.org/10.1016/j.ssc.2025.116101**

[P254-2025] "Engineering Graded Magnetic Anisotropy via Cation Interdiffusion in Core/Shell Nanoparticles"

Orozco-Henao, J. M.; **Almeida, A. A.*; Fabris, F.***; Addato, M. A. F.; Fonticelli, M. H.; **Muraca, D.***; Lavorato, G. C.

Spinel ferrite nanoparticles (NPs) with controlled composition, size, and morphology have offered a wide range of functional properties, but engineering nonhomogeneous composition profiles remains elusive. Here, we use Fe3O4/CoFe2O4 core/shell NPs as precursors to prepare compositionally graded NPs via controlled interfacial diffusion of metal cations. Electron-microscopy-based elemental mapping reveals that thermal annealing above 200 degrees C in an oxygen-rich atmosphere transforms the initially sharp core/shell interface into a compositionally graded spinel structure with a Co-rich outer layer.This cation redistribution results in pronounced changes in the magnetic properties, including a remarkable increase in coercivity and high-field susceptibility. Enhancement in the effective anisotropy is quantitatively described by modeling the time-dependent Co diffusion, enabling estimation of the cation diffusivity.These findings demonstrate a robust strategy for preparing anisotropy-graded spinel ferrite NPs, offering a broadly applicable approach to tailoring the properties of complex metal oxide nanostructures.

NANO LETTERS 25[33], p. 12645-12652, 2025. DOI: 10.1021/acs.nanolett.5c03005. **Acesso: https://doi.org/10.1021/acs.nanolett.5c03005**

[P255-2025] "Entangled Interlocked Diamond-like (Diamondiynes) Lattices"

Bastos, C. M. de O.; Santos, E. J. A. dos; Alves, R. A. F.; Dias, A. C.; Ribeiro Jr., L. A.; **Galvao, D. S.***

Diamondiynes, a new class of diamond-like carbon allotropes composed of carbon with sp/sp3-hybridized carbon networks, exhibit unique structural motifs that have not been previously reported in carbon materials. These architectures feature sublattices that are both interlocked and capable of relative movement. Using the density functional theory approach with semilocal and hybrid exchange-correlation functionals, we have conducted an extensive investigation into the structural and electronic properties of five diamondyne structures. Our results show that diamondiynes are thermodynamically stable and exhibit wide electronic band gaps, ranging from 2.2 to 4.0 eV. They are flexible yet highly resistant compared to other diamond-like structures. They have relatively small cohesive energy values, consistent with the fact that one diamondyne structure (2f-unsym) has already been experimentally realized. Our results provide new physical insights into diamond-like carbon networks and suggest promising directions for the development of porous, tunable frameworks with potential applications in energy storage and conversion.

ACS OMEGA 10[39], p. 46065-46070, 2025. DOI: 10.1021/acsomega.5c07159. **Acesso: https://doi.org/10.1021/acsomega.5c07159**

[P256-2025] "Evidence for a field-induced Lifshitz transition in the Weyl semimetal CeAlSi"

Piva, M. M.; Helm, T.; **Souza, J. C.*; Pakuszewski, K. R.*; Adriano, C.*; Pagliuso, P. G.*;** Nicklas, M.

The Weyl semimetal CeAlSi crystallizes in the noncentrosymmetric tetragonal space groupI41mdand exhibits ferromagnetic order below 8 K, thereby breaking both spatial inversion and time-reversal symmetries. This unique combination of properties establishes CeAlSi as a model system for studying the interplay between non-trivial topological states and strong electron correlations. In this work, we report observations of Shubnikov-de Haas oscillations in the electrical resistivity under magnetic fields up to 68 T applied parallel to the [001] crystallographic axis. Our measurements reveal an abrupt change in the oscillation frequencies near 14 T, which is indicative of a field-induced Lifshitz transition. Additionally, our results are consistent with the ferromagnetic order bringing the Weyl nodes closer to the Fermi level in CeAlSi. Furthermore, they suggest that the RKKY interaction plays an important role.

Journal of physics. Condensed matter : an Institute of Physics journal 37, 415704, 2025. DOI: 10.1088/1361-648X/ae0be0. **Acesso: https://iopscience.iop.org/article/10.1088/1361-648X/ae0be0**

[P257-2025] "Exploring quantum statistics for massive Dirac and Majorana neutrinos using spinor-helicity techniques"

Bigaran, I.; Parke, S. J.; **Pasquini, P.***

Recently, there has been interest in the applicability of quantum statistics to distinguish Dirac from Majorana neutrinos in multineutrino final states. In particular, debate has arisen over the validity of the Dirac-Majorana confusion theorem in these processes, i.e., that any distinction between the Dirac and Majorana processes goes to zero as the neutrino mass goes to zero. Here we approach this problem equipped with spinor-helicity methods generalized for massive Dirac and Majorana fermions. We explicitly calculate all helicity amplitudes, and their squares, for the decay of a light scalar particle to two neutrinos and two oppositely charged leptons.

This allows us to pinpoint the crucial steps which could lead to claims of a violation of the confusion theorem. We show that, if the correct antisymmetrization of Dirac to Majorana amplitudes is used, identification of which is clear in this framework, and all relevant contributions are appropriately summed, a scalar decay into two charged leptons and two neutrinos satisfies the Dirac-Majorana confusion theorem.

PHYSICAL REVIEW D 112[5], 053008, 2025. DOI: 10.1103/23ks--btx5**. Acesso: https://doi.org/10.1103/23ks-btx5**

[P258-2025] "First measurement of Ds1(1+)(2536)+ and Ds2*(2*)(2573)* production in proton-proton collisions at √s=13 TeV at the LHC"

Acharya, S.; Agarwal, A.; Guardiano, G. G.*; Jahnke, C.*; Liveraro, G. S. S.*; Takahashi, J.*; et al.
ALICE Collaboration

The production yields of the orbitally excited charm-strange mesons D(s1()1(+))(2536)(+) and D-s2*(2*)(2573)* were measured for the first time in proton-proton (pp) collisions at a center-of-mass energy of root s = 13 TeV with the ALICE experiment at the LHC. The D-s1(+) and D-s2*(+) mesons were measured at midrapidity (|y| <0.5) in minimum-bias and high-multiplicity pp collisions in the transverse-momentum interval 2 < p(T) <24 GeV/c. Their production yields relative to the D-s(+) ground--state yield were found to be compatible between minimum--bias and high-multiplicity collisions, as well as with previous measurements in e(+/-)p and e(+)e(-) collisions. The measured D-s1(+)/D-s(+) and D-s2*(+) /D-s(+) yield ratios are described by statistical hadronization models and can be used to tune the parameters governing the production of excited charm--strange hadrons in Monte Carlo generators, such as PYTHIA 8.

PHYSICAL REVIEW D 111[11], 112005, 2025. DOI: 10.1103/PhysRevD.111.112005. **Acesso: https://doi.org/10.1103/PhysRevD.111.112005**

[P259-2025] "From ionic insulator to filamentary correlated metal: Non-Fermi-liquid behavior in CuCl"

Pimentel, D. P.*

The ionic insulator copper chloride CuCl undergoes a dramatic electric-field-induced transition to a correlated metallic state, exhibiting striking non-Fermi-liquid (NFL) behavior. We demonstrate that a 70 V bias applied to compressed CuCl pellets triggers resistive switching from highly insulating 10(6) Omega to metallic 10(3) Omega states at room temperature, accompanied by characteristic non-linear I-V curves showing (i) hysteresis upon cycling and (ii) a 33 V threshold for electronic reordering. This transition is attributed to metallic copper filament formation via solid-state electrolysis, creating a heterogeneous system where the I-V evolution confirms competing processes: filament growth (ohmic -> metallic) and oxidative degradation (non-linear -> insulating). Temperature-dependent resistance in the metallic state reveals anomalous power-law behavior (R similar to T-alpha, alpha = 1.2-2.1), deviating from Fermi-liquid expectations (alpha = 2). Magnetoresistance shows a crossover from negative (T < 60 K) to positive (T > 60 K) regimes, indicating competition between weak localization and spin scattering. Oxidation to Cu2Cl(OH)(3) introduces magnetic interactions that further modulate transport. The I-V characteristics' dependence on cycling and threshold voltages establishes CuCl as a tunable platform for NFL phenomena, bridging ionic insulators and correlated conductors through electrochemically gated filamentary networks.

JOURNAL OF APPLIED PHYSICS 138[11], 115105, 2025. DOI: 10.1063/5.0282180. **Acesso: https://doi.org/10.1063/5.0282180**

[P260-2025] "Higher-order symmetry plane correlations in Pb-Pb collisions at √sNN=5.02 TeV"

Acharya, S.; Agarwal, A.; **Guardiano, G. G.*; Jahnke, C.*; Liveraro, G. S. S.*; Takahashi, J.*;** et al.
ALICE Collaboration

The correlations between event-by-event fluctuations of symmetry planes are measured in Pb-Pb collisions at a center-of--mass energy per nucleon pair root sNN = 5.02 TeV recorded by the ALICE detector at the Large Hadron Collider. This analysis is conducted using the Gaussian estimator technique, which is insensitive to biases from correlations between different flow amplitudes. The study presents, for the first time, the centrality dependence of correlations involving up to five different symmetry planes. The correlation strength varies depending on the harmonic order of the symmetry plane and the collision centrality. Comparisons with measurements from lower energies indicate no significant differences within uncertainties. Additionally, the results are compared with hydrodynamic model calculations. Although the model predictions provide a qualitative explanation of the experimental results, they overestimate the data for some observables. This is particularly true for correlators that are sensitive to the nonlinear response of the medium to initial-state anisotropies in the collision system. As these new correlators provide unique information-independent of flow amplitudes-their usage in future model developments can further constrain the properties of the strongly interacting matter created in ultrarelativistic heavy-ion collisions.

PHYSICAL REVIEW C 111[6], 064913, 2025. DOI: 10.1103/zx6t-29hf**. Acesso: https://doi.org/10.1103/zx6t-29hf**

[P261-2025] "Identification of low-momentum muons in the CMS detector using multivariate techniques in proton-proton collisions at √s=13.6 TeV"

Chekhovsky, V.; Hayrapetyan, A.; **Chinellato, J. A.*;** et al.
CMS Collaboration

"Soft" muons with a transverse momentum below 10 GeV are featured in many processes studied by the CMS experiment, such as decays of heavy-flavor hadrons or rare tau lepton decays. Maximizing the selection efficiency for these muons, while simultaneously suppressing backgrounds from long-lived light--flavor hadron decays, is therefore important for the success of the CMS physics program. Multivariate techniques have been shown to deliver better muon identification performance than traditional selection techniques. To take full advantage of the large data set currently being collected during Run 3 of the CERN LHC, a new multivariate classifier based on a gradient--boosted decision tree has been developed. It offers a significantly improved separation of signal and background muons compared to a similar classifier used for the analysis of the Run 2 data. The performance of the new classifier is evaluated on a data set collected with the CMS detector in 2022 and 2023, corresponding to an integrated luminosity of 62 fb(-1).

JOURNAL OF INSTRUMENTATION 20[4], P04021, 2025. DOI: 10.1088/1748-0221/20/04/P04021. **Acesso: https://iopscience.iop.org/article/10.1088/1748-0221/20/04/P04021**

[P262-2025] "Improving resectable gastric cancer prognosis prediction: A machine learning analysis combining clinical features and body composition radiomics"

Liveraro, G. S. S.*; Takahashi, M. E. S.*; Lascala, F.; Lopes, L. R.; Andreollo, N. A., Mendes, M. C. S., **Takahashi, J.***; Carvalheira, J. B. C.

We evaluate the significance of body composition radiomics in predicting outcomes for resectable gastric cancer (GC)

patients, as these parameters can enhance optimal surveillance strategies and risk-stratification models. Automated segmentation using deep learning algorithms was employed on CT images to analyze body composition in 276 GC patients, retrospectively recruited from the Clinical Hospital of the University of Campinas. Radiomics features of skeletal muscle (SM), visceral adipose tissue (VAT), and subcutaneous adipose tissue (SAT) were calculated. Body composition radiomics were integrated with clinicopathological factors using machine learning (ML) algorithms trained for patient outcome prediction. We compared results using Random Forest, Logistic Regression and Boosted Decision Tree algorithms. To identify the relevant features for the prognosis, recursive feature inclusion (RFI) was performed using SHAP Importance ranking. Our study uncovered novel body composition radiomic features that enhance patient prognosis, particularly the 90th percentile radiodensity value (HU) for SM and VAT. The ML model output also refined pathological staging: Stage II patients with a higher predicted mortality risk by the model had overall survival (OS) similar to Stage III patients, while Stage III patients with lower predicted risk showed OS comparable to Stage II. This approach demonstrates that the integration of clinical and radiomic features enhances the accuracy of pathological staging and offers more detailed information to refine treatment strategies for gastric cancer patients. Skeletal muscle and visceral adipose tissue radiodensity percentiles emerged as crucial determinants of patient outcomes.

INFORMATICS IN MEDICINE UNLOCKED 52, 101608, 2025. DOI: 10.1016/j.imu.2024.101608. **Acesso: https://doi.org/10.1016/j.imu.2024.101608**

[P263-2025] "Influence of Tissue Curvature on the Absolute Quantification in Frequency-Domain Diffuse Optical Spectroscopy"

Martins, G. G.*; Forti, R. M.; **Mesquita, R. C.***

Accurate estimation of optical properties and hemodynamic parameters is critical for advancing frequency-domain diffuse optical spectroscopy (FD-DOS) techniques in clinical neuroscience. However, conventional FD-DOS models often assume planar air–tissue interfaces, introducing errors in anatomically curved regions such as the forehead or infant heads. This study evaluates the impact of incorporating tissue curvature into forward models for FD-DOS analysis. Using simulations and optical phantoms, we demonstrate that curved models reduce errors in absorption coefficient estimation from 20% to less than 10% in high-curvature scenarios. Within the curvatures tested, even minor curvature mismatches resulted in errors significantly lower than those observed from planar approximations ($p < 0.001$). In low-curvature regions, curved models yielded errors comparable to planar models (<5% in both cases). When applied to human data, our proposed curved model increased absorption and hemoglobin concentration estimates by 10–15% compared to standard semi-infinite models, closer to physiological expectations. Overall, these results quantitatively demonstrate that accounting for tissue curvature in FD-DOS forward models significantly improves the accuracy of optical property estimation. We propose a numerical framework that achieves this in a fast and reliable manner, advancing FD-DOS as a robust tool for clinical and research applications in anatomically complex regions.

SPECTROSCOPY JOURNAL 3[2], 2025. DOI: 10.3390/spectroscj3020014. **Acesso: https://doi.org/10.3390/spectroscj3020014**

[P264-2025] "Integrating classical and quantum mechanics in melatonin receptors for structure-guided drug design"

Menezes, G. de L.; Silva, G. V. R. da; **Bezerra, K. S.*;** Saivish, M. V.; Dantas, C. S. G. R.; **Galvão, D. S.*;** Araújo, J. F.; Oliveira, J. I. N.; Silva, R. A. da; Fulco, U. L.

Although melatonin receptor agonists are acknowledged for their therapeutic potential for managing sleep problems, the structural optimization of these compounds is made challenging by variations in crystallographic data. This study aims to improve the structure of the melatonin receptor type 1 and ramelteon (MT1-RMT) complex and propose a new melatonin receptor agonist with an enhanced binding affinity. Molecular dynamics (MD) simulations have been used to improve the experimental MT1-RMT complex, followed by quantum-mechanical (QM) calculations employing density functional theory (DFT) to assess ligand–receptor interactions. The MD simulations effectively optimized the MT1-RMT complex, resulting in a conformation that was consistent with the experimental binding affinities. The QM calculations validated the improved binding affinity, and additional structural insights facilitated the rational design of a new agonist, N-[2-(5-methoxy-2-phenyl-1H-indol-3-yl)ethyl]propanamide (MPI), which exhibited better affinity for the MT1 and melatonin receptor type 2 (MT2) receptors. These findings suggest that MD-based refinement enhances the precision of protein–ligand complex models and that MPI is a suitable candidate for future pharmaceutical development. Subsequent research should examine the pharmacokinetic characteristics and in vivo effectiveness of MPI.

ACADEMIA BIOLOGY 3[3], 2025. DOI: 10.20935/AcadBiol7907. **Acesso: https://www.academia.edu/2837-4010/3/3/10.20935/AcadBiol7907**

[P265-2025] "Inference of the Mass Composition of Cosmic Rays with Energies from 1018.5 to 1020 eV Using the Pierre Auger Observatory and Deep Learning"

Halim, A. A.; Abreu, P.; **Bonneau Arbeletche, L.*; Chinellato, J. A.*; Dobrigkeit, C.*; Fauth, A. C.*; Machado Payeras, A.*; Reginatto Akim, J. V.*;** et al.
Pierre Auger Collaboration

We present measurements of the atmospheric depth of the shower maximum X-max, inferred for the first time on an event-by-event level using the surface detector of the Pierre Auger Observatory. Using deep learning, we were able to extend measurements of the X-max distributions up to energies of 100 EeV (10(20) eV), not yet revealed by current measurements, providing new insights into the mass composition of cosmic rays at extreme energies. Gaining a 10-fold increase in statistics compared to the fluorescence detector data, we find evidence that the rate of change of the average X-max with the logarithm of energy features three breaks at 6.5 +/- 0.6(stat) +/- 1(syst) EeV, 11 +/- 2(stat)+/- 1(syst)EeV, and 31 +/- 5(stat)+/- 3(syst) EeV, in the vicinity to the three prominent features (ankle, instep, suppression) of the cosmic-ray flux. The energy evolution of the mean and standard deviation of the measured X-max distributions indicates that the mass composition becomes increasingly heavier and purer, thus being incompatible with a large fraction of light nuclei between 50 and 100 EeV.

PHYSICAL REVIEW LETTERS 134[2], 021001, 2025. DOI: 10.1103/PhysRevLett.134.021001. **Acesso: https://doi.org/10.1103/PhysRevLett.134.021001**

[P266-2025] "Interfacial Water Dielectric Constant in the Parallel Direction to Its Surface: A Measuring Technique"

Teschke, O.*; Gomes, W. E.; **Soares, D. M.***

The dielectric constant of interfacial water was recently measured in the normal direction to the water surface; this study showed a significant reduction to a value as low as epsilon similar to 3. Here, a technique that measures parallel to the water surface dielectric constant is described.

An asymmetric arrangement of electrodes results in a configuration in which surface and bulk charging effects are separated. The water surface is responsible for the initial fast charge rearrangement. Parallel to the water surface, values as low as epsilon approximate to 35-40 were measured in agreement with models that show that this similar to 50% reduction is associated with the interfacial water confined structure.

ACS OMEGA 10[36], p. 41688-41692, 2025. DOI: 10.1021/acsomega.5c05531. **Acesso: https://doi.org/10.1021/acsomega.5c05531**

[P267-2025] "Low-Energy Cathodoluminescence of Type-I CdSe/ZnCdS Quantum Dots"

Oliveira, W. K. C. de*; Ruano Merchan, C.*; Reis, L. A.*; Park, J. W.; Bae, W. K.; **Padilha, L. A.*; Zagonel, L. F.***

Quantum dots (QDs) are a cornerstone of modern nanotechnology due to their unique optical properties. In this study, we investigate excitation dynamics in II-VI core-shell QDs under high carrier injection conditions using low-energy cathodoluminescence (CL) in a scanning tunnelling microscope (STM) setup. This approach enables spatially confined excitation of a limited number of QDs and access to higher-order excitonic states. We find that electron energies of at least 130 eV are required to induce luminescence, with no emission observed below this threshold. In QDs with thin shells (1.2 nm), increasing excitation energy modifies both luminescence intensity and spectral features, indicating altered carrier distributions and multiexciton processes in the core. In contrast, QDs with thicker shells (4.2 nm) exhibit predominantly single-exciton emission under the same conditions, consistent with reduced electron reach and carrier generation in the core. The results are compared with low-power continuous-wave photoluminescence (cw-PL), revealing distinct excitation pathways and charge dynamics. Prolonged electron exposure leads to a significant decrease in CL intensity without spectral shift or broadening, suggesting blinking behavior likely caused by charging of the QD shell. These findings provide new insight into energy deposition, carrier recombination, and beam-induced effects in core-shell QDs under localized excitation conditions.

JOURNAL OF PHYSICAL CHEMISTRY C 129[33], p. 14949-14957, 2025. DOI: 10.1021/acs.jpcc.5c04198. **Acesso: https://doi.org/10.1021/acs.jpcc.5c04198**

[P268-2025] "Luminescence and structural properties of annealed and natural blue and green Kyanite"

Costa, J. C. O.; **Fabris, F.*;** Rettori, D.; Marques, A. P. de A.; Teixeira, F. G.; Umisedo, N. K.; Nunes, M. C. dos S.; Trindade, N. M.; Yoshimura, E. M.; **Garcia-Flores, A. F.*;** Chithambo, M.; Künzel, R.

Kyanite (Al2SiO5) is an aluminum silicate with a triclinic crystal structure and occurs naturally in various colors due to trace impurities. This study evaluates the structural and luminescent properties of natural and annealed, at 1100 degrees C for 1 hour, green and blue kyanite samples. The natural and annealed samples were characterized using X-ray diffraction (XRD), Raman spectroscopy, Fourier-transform infrared spectroscopy (FTIR), ultraviolet-visible (UV-Vis) absorption, photoluminescence (PL), thermogravimetric analysis (TGA), thermoluminescence (TL), and optically stimulated luminescence (OSL). X-ray fluorescence (XRF) analysis identified several impurities, including Fe, Ca, Ti, V, and Cr, with distinct concentrations in the blue and green samples. XRD, FTIR, and Raman results confirmed the preservation of the triclinic structure after annealing, with minor distortions attributed to changes in structural order. The optical absorption data revealed significant differences between blue and green samples, particularly in the iron-related charge transfer bands. Cr3+ emissions observed in the PL spectra appeared more prominently in blue kyanite and showed high sensitivity to thermal treatment. The TL glow curves exhibited a profile with emission from 300 to 400 K for all the samples. The results indicate that annealing increases the OSL signal and induces a faster decay profile, suggesting that the thermal treatment contributes to the creation or activation of optically active trapping centers. The outcomes highlight the influence of trace impurity type, oxidation states, and concentration on the luminescent behavior of kyanite, supporting its potential applications in radiation dosimetry, luminescence dating, and optical sensing technologies.

JOURNAL OF LUMINESCENCE 288, 121506, 2025. DOI: 10.1016/j.jlumin.2025.121506. **Acesso: https://doi.org/10.1016/j.jlumin.2025.121506**

[P269-2025] "Magnetic properties and dipolar interactions of Fe3O4 nanoparticle clusters produced by bottom-up self-assembly"

Fabris, F.*; Almeida, A. A.*; Ribeiro, P. R. T.*; Pirota, K. R.*; Muraca, D.*

Magnetic nanoparticles (MNPs) exhibit unique magnetic behaviors that make them highly applicable in various fields such as biomedical technology, energy, and sensing. This study investigates the magnetic properties and dipolar interactions of Fe3O4 nanoparticle clusters with different average sizes (27.4 nm, 79.2 nm, and 112.9 nm) produced by an emulsion-based bottom-up self-assembly process. The MNPs, with an individual size of 9.8 nm, were organized into clusters, and their collective magnetic properties were explored using detailed DC and AC magnetic studies. We applied a phenomenological mean-field model to describe the magnetic behavior of the clusters, including an increase in blocking temperature, energy barriers, and relaxation dynamics as a function of cluster size. The results indicate a significant influence of dipolar interactions on the energy barriers and magnetic moment dynamics, with larger clusters exhibiting stronger dipolar fields. Our findings provide insights into the interaction between nanoparticle arrangement and magnetic properties, which offers potential for the development of novel magnetic materials for advanced applications.

JOURNAL OF MATERIALS CHEMISTRY C 13[19], p. 9756-9767, 2025. DOI: 10.1039/d5tc00022j. **Acesso: https://doi.org/10.1039/D5TC00022J**

[P270-2025] "Magnetostriction as the origin of the magnetodielectric effect in La2CoMnO6"

Boldrin, M.; Bagri, A.; Barlettani, D.; Teather, E.; Squillante, L.; Souza, M. de; Pontes, R. B.; Silva, A. G.; Mori, T. J. A.; Perry, R.; Lora-Serrano, R.; **Granado, E.*;** Bittar, E. M.; Veiga, L. S. I.; Bufaical, L.

The La2CoMnO6 (LCMO) perovskite has received a lot of attention due to its near-room-temperature magnetodielectric effect. Despite the recent efforts, the mechanism ruling the correlation between its magnetic and dielectric properties is not yet fully understood. In order to address this issue, we conducted a detailed investigation of the coupling between the structural, electronic, and magnetic properties of a polycrystalline LCMO sample. Using magnetic field-dependent x-ray powder diffraction and measurements with a capacitive dilatometer, we show that applying an external magnetic field decreases the unit cell volume, thereby modifying the octahedral distortions. Experiments involving temperature and field-dependent x-ray absorption spectroscopy at the Co-L2,3 edges provide further evidence that the spin-orbit interaction of outermost Co 3d orbital and the field-induced enhancement of covalence effects are the key contributors to the magnetostrictive effects.

From a detailed analysis using multiplet and density functional theory calculations, we propose that the field-induced modulations of the orbital hybridization and the ligand-to-metal charge transfer are responsible for the changes in the dielectric response of LCMO, thus enabling a direct coupling between magnetic, elastic, and dielectric properties in this material.

PHYSICAL REVIEW MATERIALS 9[9], 094403, 2025. DOI: 10.1103/sjr4-6kdp. **Acesso: https://doi.org/10.1103/sjr4--6kdp**

[P271-2025] "Maximal value for trilinear Higgs coupling in a 3-3-1 EFT"

Cherchiglia, A.*; Leite, L. J. F.*

Recent efforts, both theoretical and experimental, have increasingly focused on the scalar potential of the Standard Model, with a highlight on the trilinear Higgs coupling. This parameter has long been recognized for its potential to test Beyond-Standard--Model (BSM) theories and its significance in understanding early cosmological dynamics.In order to broadly map BSM scenarios, a powerful tool is to devise its effective field theory (EFT) version for low-energies. In this work, we obtain a consistent EFT for a class of models based on the gauge group SU(3)c x SU(3)L x U(1) Y. After properly matching the UV-complete theory at one-loop, we show that the EFT is a Two-Higgs-Doublet Model (2HDM), where some of the quartic couplings are naturally small. By imposing bounds from electroweak precision observables, collider, flavor, as well as theoretical considerations, we obtain that the maximum value of the trilinear Higgs coupling is more than four times larger than the SM prediction, potentially testable at the LHC Hi-Lumi upgrade and other future colliders. Moreover, we find that such large values are only attainable if one considers an out-of-alignment scenario, even if the deviation is very small.

JOURNAL OF HIGH ENERGY PHYSICS [9], 101, 2025. DOI: 10.1007/JHEP09(2025)101. **Acesso: https://doi.org/10.1007/JHEP09(2025)101**

[P272-2025] "Measurement of the inclusive cross sections for W and Z boson production in proton-proton collisions at √s=5.02 and 13 TeV"

Hayrapetyan, A.; Tumasyan, A.; **Chinellato, J. A.*;** et al.
CMS Collaboration

Measurements of fiducial and total inclusive cross sections for W and Z boson production are presented in proton-proton collisions at root s = 5.02 and 13TeV. Electron and muon decay modes (l = e or mu) are studied in the data collected with the CMS detector in 2017, in dedicated runs with reduced instantaneous luminosity. The data sets correspond to integrated luminosities of 298 +/- 6 pb(-1) at 5.02TeV and 206 +/- 5 pb(-1) at 13TeV. Measured values of the products of the total inclusive cross sections and the branching fractions at 5.02TeV are sigma(pp -> W+ X)B(W -> l nu) = 7300 +/- 10 (stat) +/- 60 (syst) +/- 140 (lumi) pb, and sigma(pp -> Z+ X)B(Z -> l(+) l(-)) = 669 +/- 2 (stat)+/- 6 (syst)+/- 13 (lumi) pb for the dilepton invariant mass in the range of 60-120 GeV. The corresponding results at 13TeV are 20480 +/- 10 (stat)+/- 170 (syst)+/- 470 (lumi) pb and 1952 +/- 4 (stat)+/- 18 (syst)+/- 45 (lumi) pb. The measured values agree with cross section calculations at next-to-next-to-leading-order in perturbative quantum chromodynamics. Fiducial and total inclusive cross sections, ratios of cross sections of W+ and W- production as well as inclusive W and Z boson production, and ratios of these measurements at 5.02 and 13TeV are reported.

JOURNAL OF HIGH ENERGY PHYSICS [4], 162, 2025. DOI: 10.1007/JHEP04(2025)162. **Acesso: https://doi.org/10.1007/JHEP04(2025)162**

[P273-2025] "Measurement of the inclusive isolated-photon production cross section in pp and Pb-Pb collisions at √sNN=5.02 TeV"

Acharya, S.; Agarwal, A.; **Guardiano, G. G.*; Jahnke, C.*; Liveraro, G. S. S.*; Takahashi, J.***; et al.
ALICE Collaboration

The ALICE Collaboration at the CERN LHC has measured the inclusive production cross section of isolated photons at midrapidity as a function of the photon transverse momentum (p(T)(gamma)), in Pb-Pb collisions in different centrality intervals, and in pp collisions, at centre-of-momentum energy per nucleon pair of root s(NN) = 5.02 TeV. The photon transverse momentum range is between 10-14 and 40-140 GeV/c, depending on the collision system and on the Pb-Pb centrality class. The result extends to lower p(T)(gamma) than previously published results by the ATLAS and CMS experiments at the same collision energy. The covered pseudorapidity range is |eta(gamma)| < 0.67. The isolation selection is based on a charged particle isolation momentum threshold p(T)(iso,ch)=1.5 GeV/c within a cone of radii R=0.2 and 0.4. The nuclear modification factor is calculated and found to be consistent with unity in all centrality classes, and also consistent with the HG-PYTHIA model, which describes the event selection and geometry biases that affect the centrality determination in peripheral Pb-Pb collisions. The measurement is compared to next-to-leading order perturbative QCD calculations and to the measurements of isolated photons and Z(0) bosons from the CMS experiment, which are all found to be in agreement.

EUROPEAN PHYSICAL JOURNAL C 85[5], 553, 2025. DOI: 10.1140/epjc/s10052-025-13971-y. **Acesso: https://doi.org/10.1140/epjc/s10052-025-13971-y**

[P274-2025] "Measurement of the production cross section of prompt Ξc0 baryons in p-Pb collisions at √sNN=5.02 TeV"

Acharya, S.; Adamova, D.; **Chinellato, D. D.*; Guardiano, G. G.*; Jahnke, C.*; Liveraro, G. S. S.*; Takahashi, J.*;** et al.
ALICE Collaboration

The transverse momentum (p(T)) differential production cross section of the promptly produced charmstrange baryon Xi(0)(c) (and its charge conjugate <(Xi(0)(c))over bar>) is measured at midrapidity via its hadronic decay into pi(+)Xi(-) in p-Pb collisions at a centre-of-mass energy per nucleon-nucleon collision root s(NN) = 5.02 TeV with the ALICE detector at the LHC. The Xi(0)(c) nuclear modification factor (R-pPb), calculated from the cross sections in pp and p-Pb collisions, is presented and compared with the RpPb of Lambda(+)(c) baryons. The ratios between the p(T)-differential production cross section of Xi(0)(c) baryons and those of D-0 mesons and Lambda(+)(c) baryons are also reported and compared with results at forward and backward rapidity from the LHCb Collaboration. Themeasurements of the production cross section of prompt Xi(0)(c) baryons are compared with a model based on perturbative QCD calculations of charm-quark production cross sections, which includes only cold nuclear matter effects in p-Pb collisions, and underestimates the measurement by a factor of about 50. This discrepancy is reduced when the data is compared with a model that includes string formation beyond leading-colour approximation or in which hadronisation is implemented via quark coalescence. The p(T)-integrated cross section of prompt Xi(0)(c)--baryon production at midrapidity extrapolated down to p(T) = 0 is also reported. These measurements offer insights and constraints for theoretical calculations of the hadronisation process. Additionally, they provide inputs for the calculation of the charm production cross section in p-Pb collisions at midrapidity.

EUROPEAN PHYSICAL JOURNAL C 85[1], 86, 2025. DOI: 10.1140/epjc/s10052-024-13531-w. **Acesso: https://doi.org/10.1140/epjc/s10052-024-13531-w**

[P275-2025] "Measurement of ω meson production in pp collisions at √s=13 TeV"

Acharya, S.; Adamova, D.; **Chinellato, D. D.*; Guardiano, G. G.*; Jahnke, C.*; Liveraro, G. S. S.*; Takahashi, J.*;** et al.
ALICE collaboration

The p(T)-differential cross section of omega meson production in pp collisions at root s = 13 TeV at midrapidity (vertical bar y vertical bar < 0.5) was measured with the ALICE detector at the LHC, covering an unprecedented transverse-momentum range of 1.6 < p(T)< 50 GeV/c. The meson is reconstructed via the omega -> pi(+)pi(-)pi(0) decay channel. The results are compared with various theoretical calculations: PYTHIA8.2 with the Monash 2013 tune overestimates the data by up to 50%, whereas good agreement is observed with Next-to-Leading Order (NLO) calculations incorporating omega fragmentation using a broken SU(3) model. The omega/pi(0) ratio is presented and compared with theoretical calculations and the available measurements at lower collision energies. The presented data triples the p(T) ranges of previously available measurements. A constant ratio of C-omega/pi 0 = 0.578 +/- 0.006 (stat.) +/- 0.013 (syst.) is found above a transverse momentum of 4 GeV/c, which is in agreement with previous findings at lower collision energies within the systematic and statistical uncertainties.

JOURNAL OF HIGH ENERGY PHYSICS [4], 067, 2025. DOI: 10.1007/JHEP04(2025)067. **Acesso: https://doi.org/10.1007/JHEP04(2025)067**

[P276-2025] "Measurements of the Higgs boson production cross section in the four-lepton final state in proton-proton collisions at √s=13.6 TeV"

Chekhovsky, V.; Hayrapetyan, A.; **Chinellato, J. A.*;** et al.
CMS Collaboration

The measurements of the Higgs boson (H) production cross sections performed by the CMS Collaboration in the four-lepton (4l, l = e, mu) final state at a center-of-mass energy root s = 13.6 TeV are presented. These measurements are based on data collected with the CMS detector at the CERN LHC in 2022, corresponding to an integrated luminosity of 34.7 fb(-1). Cross sections are measured in a fiducial region closely matching the experimental acceptance, both inclusively and differentially, as a function of the transverse momentum and the absolute value of the rapidity of the four-lepton system. The H -> ZZ -> 4l inclusive fiducial cross section is measured to be 2.89(-0.49)(+0.53) (stat)(-0.21)(+0.29) (syst) fb, in agreement with the standard model expectation of 3.09(-0.24)(+0.27)fb.

JOURNAL OF HIGH ENERGY PHYSICS [5], 079, 2025. DOI: 10.1007/JHEP05(2025)079**. Acesso: https://doi.org/10.1007/JHEP05(2025)079**

[P277-2025] "Medium-induced modification of groomed and ungroomed jet mass and angularities in Pb-Pb collisions at √sNN=5.02 TeV"

Acharya, S.; Agarwal, A.; **Guardiano, G. G.*; Jahnke, C.*; Liveraro, G. S. S.*; Takahashi, J.*;** et al.
ALICE Collaboration

The ALICE Collaboration presents a new suite of jet substructure measurements in Pb-Pb and pp collisions at a center-of-mass energy per nucleon pair root s(NN) = 5.02 TeV. These measurements provide access to the internal structure of jets via the momentum and angle of their constituents, probing how the quark--gluon plasma modifies jets, an effect known as jet quenching. Jet grooming additionally removes soft wide-angle radiation to enhance perturbative accuracy and reduce experimental uncertainties.We report the groomed and ungroomed jet mass m(jet) and jet angularities lambda(kappa)(alpha) using kappa = 1 and alpha > 0. Charged-particle jets are reconstructed at midrapidity using the anti-k(T) algorithm with resolution parameter R = 0.2. A narrowing of the jet mass and angularity distributions in Pb-Pb collisions with respect to pp is observed and is enhanced for groomed results, confirming modification of the jet core. By using consistent jet definitions and kinematic cuts between the mass and angularities for the first time, previous inconsistencies in the interpretation of quenching measurements are resolved, rectifying a hurdle for understanding how jet quenching arises from first principles and highlighting the importance of a well--controlled baseline. These results are compared with a variety of theoretical models of jet quenching, providing constraints on jet energy-loss mechanisms in the quark-gluon plasma.

PHYSICS LETTERS B 864, 139409, 2025. DOI: 10.1016/j.physletb.2025.139409. **Acesso: https://doi.org/10.1016/j.physletb.2025.139409**

[P278-2025] "Metal-Electrolyte-Semiconductor Capacitors to Quantify Interface State Density in Printed ZnO for Low--Voltage UV Photodetectors"

Vieira, D. H.; Nogueira, G. L.; **Oliveira, R. F. de*;** Gomes, H. L.; Alves, N.

This study reports the fabrication and electrical characterization of metal-electrolyte-semiconductor (MES) capacitors based on printed ZnO as a semiconducting layer and a cellulose-based eco-friendly electrolyte. The results demonstrate that MES capacitors behave similarly to their solid-state metal-insulator--semiconductor (MIS) counterparts. Capacitance-voltage measurements show well-defined charge saturation and depletion plateaus, and the Mott-Schottky plots exhibit the expected linear behavior, allowing the extraction of the semiconductor free carrier density. Upon UV light exposure with varying irradiance, the flat-band voltage shifts consistently with a light--induced increase in free carrier density, and the capacitance increases due to trap filling. These behaviors are confirmed by measurements using a phototransistor structure. The frequency response of the MES capacitors also reveals low-frequency relaxation peaks in the capacitance spectrum, which align with a continuous distribution of interface state density reaching approximately similar to 4.86 x 1013 cm-2<middle dot>eV-1. These findings confirm that MES capacitors can effectively quantify electronic states at the electrolyte/semiconductor interface. This capability, along with a high capacitance ratio [C light - C dark]/C dark at very low voltages, is particularly valuable for applying MES devices in a wide range of sensing applications, especially in field-effect photodetectors.

ACS APPLIED ELECTRONIC MATERIALS 7[17], p. 8180-8190, 2025. DOI: 10.1021/acsaelm.5c01263. **Acesso: https://doi.org/10.1021/acsaelm.5c01263**

[P279-2025] "Metallic Nitride Microfluidic e-Tongue: A Novel Selective Approach for the Detection of Macronutrients in Soil"

Boeira, C. D.*; Leidens, L. M.*; Costa, E. E. C.*; Gonçalves, M. H.*; Perillo, A. S.*; Ferraz, F. A.*; Marchi, M. C.; **Shimizu, F. M.***; Amaral, L. R.; **Alvarez, F.*; Riul Jr., A.***

The growing global demand for food requires optimizing agricultural practices and more rational use of natural resources without expanding cropping areas. Precision agriculture (PA) tools are essential for accurately applying fertilizers and herbicides, reducing costs, and avoiding environmental impacts. Standard macronutrient mapping methods are costly and time--consuming, limiting denser sampling collection in the field. Consequently, devices employing new materials with specific properties matching sensitivity to agricultural nutrients,

robustness to face intensive climatic variations, and economical manufacturing viability are mandatory. In this sense, microfluidic impedimetric e-tongues have emerged as practical tools in PA due to their high sensitivity, adaptability, affordability, and ease of use. These sensors provide rapid qualitative and quantitative results in liquid media, with applications extending to food analysis, environmental monitoring, and biosensing. Here, metallic nitride thin films (CrN, BN, and TiN) deposited via physical vapor deposition (PVD) using the glancing angle deposition (GLAD) technique are applied as sensing units presenting high sensitivity, controlled micro- and nanostructures, durability, reproducibility, and mechanical robustness, essential characteristics for future on-site soil analyses. The GLAD technique allows precise control over the micro- and nanostructures deposited on gold interdigitated electrodes to create molecular sieves for a possible capture of target species (e.g., K+, Na+, Mg2+, Ca2+, PO43-) from soil samples. We demonstrate the feasibility of using distinct nitrides as sensing units in a microfluidic e-tongue tested with soil samples with distinct compositions diluted in water without pretreatments. The sensor successfully differentiated all samples tested, showing higher K and Mg macronutrient resolution. These findings demonstrate the high potential to detect minute changes (<1 mmol<middle dot>L-1) in soil fertilization, with results compared by four prediction models, paving the way for future in situ analyses envisaging a controlled delivery of macronutrients during fertilization.

ACS SENSORS 10[8], p. 5760-5771, 2025. DOI: 10.1021/acssensors.5c00921. **Acesso:** **https://doi.org/10.1021/acssensors.5c00921**

[P280-2025] "Minimal Example of Quantum Nonclassicality without Freedom of Choice"

Lauand, P.*; Poderini, D.; **Rabelo, R.*;** Chaves, R.

Bell's theorem is often considered the most stringent notion of nonclassicality. The generalization of Bell's theorem to causal networks offers interesting new perspectives on the phenomenon of quantum nonclassicality and prompts us with a fundamental inquiry: what is the simplest scenario leading to the incompatibility between quantum correlations and the classical theory of causality? Here, we demonstrate that quantum nonclassicality is possible in an entanglement swapping network consisting of only three dichotomic variables, without the need for the locality assumption or external measurement choices. We also show that interventions, a central tool in the field of causal inference, significantly improve the noise robustness of this new kind of nonclassical behavior, making it feasible for experimental tests with current technology.

PHYSICAL REVIEW LETTERS 135[9], 090201, 2025. DOI: 10.1103/3854-r395. **Acesso:** **https://doi.org/10.1103/3854--r395**

[P281-2025] "Model-agnostic search for dijet resonances with anomalous jet substructure in proton-proton collisions at s=13 TeV"

Chekhovsky, V.; Hayrapetyan, A.; **Chinellato, J. A.*;** et al.
CMS Collaboration

This paper presents a model-agnostic search for narrow resonances in the dijet final state in the mass range 1.8-6 TeV. The signal is assumed to produce jets with substructure atypical of jets initiated by light quarks or gluons, with minimal additional assumptions. Search regions are obtained by utilizing multivariate machine-learning methods to select jets with anomalous substructure. A collection of complementary anomaly detection methods-based on unsupervised, weakly supervised, and semisupervised algorithms-are used in order to maximize the sensitivity to unknown new physics signatures. These algorithms are applied to data corresponding to an integrated luminosity of 138 fb-1, recorded by the CMS experiment at the LHC, at a center-of-mass energy of 13 TeV. No significant excesses above background expectations are seen. Exclusion limits are derived on the production cross section of benchmark signal models varying in resonance mass, jet mass, and jet substructure. Many of these signatures have not been previously sought, making several of the limits reported on the corresponding benchmark models the first ever. When compared to benchmark inclusive and substructure-based search strategies, the anomaly detection methods are found to significantly enhance the sensitivity to a variety of models.

REPORTS ON PROGRESS IN PHYSICS 88[6], 067802, 2025. DOI: 10.1088/1361-6633/add762. **Acesso:** **https://iopscience.iop.org/article/10.1088/1361-6633/add762**

[P282-2025] "Multiple Quasiparticle Interactions in Molecularly Functionalized h-BN Polaritonic Systems"

Pereira-Andrade, E.; Barreto, R. R.; **Bernardes, Y.*;** Barcelos, I. D.; Malachias, A.; Maia, F. C. B.; Sáfar, G. de A. M.

Spectroscopic measurements focusing on hybrid light-matter interactions have emerged as a powerful tool for exploring nanoscale energy exchange and optical confinement. Uncovering the interaction between vibrational modes of Tb(H3PTC)3 molecules and phonon-polaritons in h-BN flakes, as well as the interaction between the same polaritons with the molecular excitons of Tb(H3PTC)3, this study demonstrates the formation of hybrid modes in this system at room temperature in the infrared range. Combining h-BN crystals and molecular films, the system achieves coupling between excitons and polaritons, confirmed by near-field optical measurements in the infrared and spectral analysis. This research highlights the effective integration of molecular phonons and excitons with confined polaritonic modes, revealing the potential for efficient energy exchange in hybrid systems. The findings contribute to the broader understanding of vibrational-polaritonic interactions and underscore the utility of this straightforward platform for applications in nanospectroscopy, optoelectronics, and light-matter interaction technologies.

JOURNAL OF PHYSICAL CHEMISTRY C 129[36], p. 16147-16154, 2025. DOI: 10.1021/acs.jpcc.5c02986**. Acesso:** **https://doi.org/10.1021/acs.jpcc.5c02986**

[P283-2025] "Multiplicity dependence of charm baryon and charm meson production in pPb collisions at √SNN=8.16 TeV"

Hayrapetyan, A.; Tumasyan, A.; Adam, W.; **Chinellato, J. A.*;** et al.
CMS Collaboration

Measurements of the production yields of charm baryons (Lambda(+)(c)) and charm mesons (D-0) in proton-lead collisions at a nucleon-nucleon center-of-mass energy of 8.16 TeV are presented. The data were collected in 2016 with the CMS experiment and correspond to an integrated luminosity of 186 nb(-1). The Lambda(+)(c) baryon is reconstructed from the decay channel Lambda(+)(c) -> K(S)(0)p, while the D-0 meson is reconstructed via D-0 -> K- pi(+). The Lambda(+)(c) baryon and D-0 meson yields are extracted in several charged-particle multiplicity classes. No strong multiplicity dependence of the Lambda(+)(c) -to-D-0 yield ratio is observed, unlike the observed strange baryon to strange meson yield ratio of Lambda/(Lambda) over bar to K-S(0), which shows a strong multiplicity dependence. This observation indicates different mechanisms for the multiplicity evolution of hadronization processes for charm and strange quarks and provides new constraints to the understanding of heavy flavor production and collectivity in small collision systems.

PHYSICS LETTERS B 868, 139672, 2025. DOI: 10.1016/j.physletb.2025.139672. **Acesso: https://doi.org/10.1016/j.physletb.2025.139672**

[P284-2025] "Multiplicity-dependent jet modification from di-hadron correlations in pp collisions at √s=13 TeV"

Acharya, S.; Agarwal, A.; **Guardiano, G. G.*; Jahnke, C.*; Liveraro, G. S. S.*; Takahashi, J.*;** et al.
ALICE Collaboration

Short-range correlations between charged particles are studied via two-particle angular correlations in pp collisions at root s = 13 TeV. The correlation functions are measured as a function of the relative azimuthal angle triangle phi and the pseudorapidity separation triangle eta for pairs of primary charged particles within the pseudorapidity interval |eta| < 0.9 and the transverse-momentum range 1 < p(T) < 8 GeV/c. Near-side (|triangle phi| < 1.3) peak widths are extracted from a generalised Gaussian fitted over the correlations in full pseudorapidity separation (|triangle eta| < 1.8), while the per-trigger associated near-side yields are extracted for the short-range correlations (|triangle eta| < 1.3). Both are evaluated as a function of charged-particle multiplicity obtained by two different event activity estimators. The width of the near-side peak decreases with increasing multiplicity, and this trend is reproduced qualitatively by the Monte Carlo event generators PYTHIA 8, AMPT, and EPOS. However, the models overestimate the width in the low transverse-momentum region (p(T) < 3 GeV/c). The per-trigger associated near-side yield increases with increasing multiplicity. Although this trend is also captured qualitatively by the considered event generators, the yield is mostly overestimated by the models in the considered kinematic range. The measurement of the shape and yield of the short--range correlation peak can help us understand the interplay between jet fragmentation and event activity, quantify the narrowing trend of the near-side peak as a function of transverse momentum and multiplicity selections in pp collisions, and search for final-state jet modification in small collision systems.

JOURNAL OF HIGH ENERGY PHYSICS [3], 194, 2025. DOI: 10.1007/JHEP03(2025)194. **Acesso: https://doi.org/10.1007/JHEP03(2025)194**

[P285-2025] "Multiprobe cosmology from the abundance of SPT clusters and DES galaxy clustering and weak lensing"

Bocquet, S.; Grandis, S.; **Navarro-Alsina, A.*;** et al.
DES and SPT Collaborations

Cosmic shear, galaxy clustering, and the abundance of massive halos each probe the large-scale structure of the Universe in complementary ways. We present cosmological constraints from the joint analysis of the three probes, building on the latest analyses of the lensing-informed abundance of clusters identified by the South Pole Telescope (SPT) and of the auto- and cross-correlation of galaxy position and weak lensing measurements (3 × 2pt) in the Dark Energy Survey (DES). We consider the cosmological correlation between the different tracers and we account for the systematic uncertainties that are shared between the large-scale lensing correlation functions and the small-scale lensing-based cluster mass calibration. Marginalized over the remaining Λ cold dark matter (ΛCDM) parameters (including the sum of neutrino masses) and 52 astrophysical modeling parameters, we measure Ωm ¼ 0.300 0.017 and σ8 ¼ 0.797 0.026. Compared to constraints from Planck primary cosmic microwave background (CMB) anisotropies, our constraints are only 15% wider with a probability to exceed of 0.22 (1.2σ) for the two-parameter difference. We further obtain S8 = σ8δΩm=0.3Þ0.5 ¼ 0.796 0.013 which is lower than the Planck measurement at the 1.6σ level. The combined SPT cluster, DES 3 × 2pt, and Planck datasets mildly prefer a nonzero positive neutrino mass, with a 95% upper limit Pmv < 0.25 eV on the sum of neutrino masses. Assuming a wCDM model, we constrain the dark energy equation of state parameter w ¼ −1.15Þ0.23 −0.17 and when combining with Planck primary CMB anisotropies, we recover w ¼ −1.20Þ0.15 −0.09 , a 1.7σ difference with a cosmological constant. The precision of our results highlights the benefits of multiwavelength multiprobe cosmology and our analysis paves the way for upcoming joint analyses of next-generation datasets.

PHYSICAL REVIEW D 111, 063533, 2025. DOI: 10.1103/PhysRevD.111.063533. **Acesso: https://journals.aps.org/prd/abstract/10.1103/PhysRevD.111.063533**

[P286-2025] "Nanoscale Band Gap Modulation and Dual Moire Superlattices of Hexagonal Boron Nitride Weakly Coupled to Graphite"

Costa, F. J. R.*; Arribas, D.; Brito, T. G. L.; Cheng, T. S.; Bradford, J.; Thompson, A.; Saywell, A.; Mellor, C. J.; Beton, P. H.; Novikov, S. V.; Plo, J.; Gil, B.; Cassabois, G.; **Zagonel, L. F.***; Kuhnke, K.; Kern, K.; Roslawska, A.

Van der Waals (vdW) materials, such as hexagonal boron nitride (h-BN), are highly promising for applications in optoelectronics and quantum technologies. When assembled into heterostructures, h-BN can form moire superlattices, enabling the engineering of electronic and optical properties by varying the interlayer twist angle. However, understanding the nanoscale interplay between moire patterns and electronic properties such as the band gap or work function, particularly in optically active h-BN structures, remains a challenge. Here, we use the atomic-scale precision of scanning tunneling microscopy (STM) to uncover the role of moire superlattices in the electronic properties of a weakly coupled h-BN/Graphite heterostructure. Our STM study reveals large moire patterns (14.8-18.3 nm periodicity) on the surface, implying slight local variations in the h-BN/Graphite stacking throughout the sample. Spectroscopic measurements show significant modulations of 330 meV in the local work function and 170 meV in the band gap within a moire unit cell, which are comparable to h-BN/metallic interfaces. Additionally, we identify dual moire superlattices in twisted homobilayers of h-BN/Graphite, offering an extra degree of freedom to tune the heterostructure's properties. These findings suggest that moire engineering in h-BN-based systems could lead to a range of effects, including exciton broadening, twist--tunable defect luminescence, and the theoretically predicted trapping of excitons within the moire landscape. Furthermore, this tunability may also affect adjacent layered materials, providing a versatile platform for tailoring the electronic and optical properties of h-BN and its van der Waals heterostructures.

ACS NANO, 2025. DOI: 10.1021/acsnano.5c09374. Early Access Date: OCT 2025. **Acesso: https://doi.org/10.1021/acsnano.5c09374**

[P287-2025] "Observation of nuclear modification of energy--energy correlators inside jets in heavy ion collisions"

Chekhovsky, V.; Hayrapetyan, A.; **Chinellato, J. A.*; et al.**
CMS Collaboration

Energy-energy correlators are constructed by averaging the number of charged particle pairs within jets, weighted by the product of their transverse momenta, as a function of the angular separation of the particles within a pair. They are sensitive to a multitude of perturbative and nonperturbative quantum chromodynamics phenomena in high-energy particle collisions. Using lead-lead data recorded with the CMS detector, energy-energy correlators inside high transverse momentum jets are measured in heavy ion collisions for the first time.

The data are obtained at a nucleon-nucleon center-of-mass energy of 5.02TeV and correspond to an integrated luminosity of 1.70 nb(-1). A similar analysis is done for proton-proton collisions at the same center-of-mass energy to establish a reference. The ratio of lead-lead to proton-proton energy-energy correlators reveals significant jet substructure modifications in the quark--gluon plasma. The results are compared to different models that incorporate either color coherence or medium response effects, where the two effects predict similar substructure modifications.

PHYSICS LETTERS B 866, 139556, 2025. DOI: 10.1016/j.physletb.2025.139556. **Acesso: https://doi.org/10.1016/j.physletb.2025.139556**

[P288-2025] "Passive demultiplexed two-photon state generation from a quantum dot"

Karli, Y.; Arenas, I. A.; Schimpf, C.; Garcia Jr., A. J.; Manna, S.; Kappe, F.; Schwarz, R.; Undeutsch, G.; Aigner, M.; Peter, M.; **Silva, S. F. C. da*;** Rastelli, A.; Weihs, G.; Remesh, V.

High-purity multi-photon states are essential for photonic quantum computing. Among existing platforms, semiconductor quantum dots offer a promising route to scalable and deterministic multi-photon state generation. However, to fully realize their potential, we require a suitable optical excitation method. Current approaches to multi-photon generation rely on active polarization-switching elements (e.g., electro-optic modulators, EOMs) to spatio-temporally demultiplex single photons. Yet, the achievable multi-photon rate is fundamentally limited by the switching speed of the EOM. Here, we introduce a fully passive demultiplexing technique that leverages a stimulated two-photon excitation process to achieve switching rates only limited by the quantum dot lifetime. We demonstrate this method by generating two-photon states from a single quantum dot without requiring active switching elements. Our approach significantly reduces the cost of demultiplexing while shifting it to the excitation stage, enabling loss-free demultiplexing and effectively doubling the achievable multi-photon generation rate when combined with existing active demultiplexing techniques.

NPJ QUANTUM INFORMATION 11[1], 139, 2025. DOI: 10.1038/s41534-025-01083-0. **Acesso: https://doi.org/10.1038/s41534-025-01083-0**

[P289-2025] "Perfect transfer of entanglement and quantum steering via parametric frequency converter"

Sohail, A.*; Hidki, A.; Nawaz, A.; Ali, H.; Ahmed, R.; **Oliveira, M. C. de***

We study the effects of a parametric frequency converter (PFC) in a two-mode cavity system where one of the cavity modes is coupled with yttrium iron garnet (YIG). The PFC acts as a nonlinear source for enhancing quantum correlations, which strongly depend on the parametric coupling and the associated phase factor. It is fascinating that the perfect transfer of entanglement and steering of various mode pairs can be achieved by adjusting the system's parameters, such as cavity--magnon coupling, gain, and the phase of the PFC. In addition, the generated entanglements in the present system are more robust against thermal effects, particularly with the inclusion of the PFC, compared to the bare-cavity case. Another intriguing finding is that phonon-cavity one-way steering appears only when magnon-cavity one-way steering completely vanishes. Our protocol for these transferring processes suggests a different approach to the processing and storage of quantum information. Graphic AbstractDescription We study the enhancement of quantum correlation and perfect transfer of entanglement of indirectly coupled modes via a parametric frequency converter (PFC) in a two-mode magnomechanical system. It is fascinating that the perfect transfer of entanglement and steering of various mode pairs can be achieved by adjusting the system's parameters, such as cavity-magnon coupling, gain, and the phase of the PFC.

EUROPEAN PHYSICAL JOURNAL D 79[9], 113, 2025. DOI: 10.1140/epjd/s10053-025-01066-y**. Acesso: https://doi.org/10.1140/epjd/s10053-025-01066-y**

[P290-2025] "Potassium decoration on graphenyldiene monolayer for advanced reversible hydrogen storage"

Laranjeira, J. A. S.; Martins, N. F.; **Lima, K. A. L.***; Aparicio--Huacarpuma, B. D.; Ribeiro Jr., L. A.; Chen, X.; **Galvao, D. S.***; Sambrano, J. R.

Potassium-decorated graphenyldiene (K@GPD) is investigated as a promising two-dimensional material for reversible hydrogen storage using first-principles density functional theory calculations. Potassium atoms bind strongly to the GPD monolayer, and ab initio molecular dynamics (AIMD) simulations confirm the thermal stability of the functionalized system at 300 K. Hydrogen adsorption energies range from-0.11 to-0.14 eV per H2, denoting reversible storage. At full coverage (18 H2 molecules), the system reaches a storage capacity of 8.82 wt%, exceeding the U.S. DOE target. AIMD simulations reveal spontaneous H2 desorption at ambient temperature, demonstrating excellent reversibility.

COMPUTATIONAL AND THEORETICAL CHEMISTRY 1254, 115504, 2025. DOI: 10.1016/j.comptc.2025.115504**. Acesso: https://doi.org/10.1016/j.comptc.2025.115504**

[P291-2025] "Proton reconstruction with the TOTEM Roman pot detectors for high-ß* LHC data"

Hayrapetyan, A.; Tumasyan, A.; **Chinellato, J. A.***; et al. CMS Collaboration; TOTEM Collaboration

The TOTEM Roman pot detectors are used to reconstruct the transverse momentum of scattered protons and to estimate the transverse location of the primary interaction. This paper presents new methods of track reconstruction, measurements of strip-level detection efficiencies, cross-checks of the LHC beam optics, and detector alignment techniques, along with their application in the selection of signal collision events. The track reconstruction is performed by exploiting hit cluster information through a novel method using a common polygonal area in the intercept-slope plane. The technique is applied in the relative alignment of detector layers with mu m precision. A tag-and-probe method is used to extract strip-level detection efficiencies. The alignment of the Roman pot system is performed through time-dependent adjustments, resulting in a position accuracy of 3 mu m in the horizontal and 60 mu m in the vertical directions. The goal is to provide an optimal reconstruction tool for central exclusive physics analyses based on the high-beta* data-taking period at root s = 13 TeV in 2018.

JOURNAL OF INSTRUMENTATION 20[4], P04012, 2025. DOI: 10.1088/1748-0221/20/04/P04012. **Acesso: https://iopscience.iop.org/article/10.1088/1748-0221/20/04/P04012**

[P292-2025] "Reciprocating thermal behavior and thermometry studies of Tb3+- and Gd3+-oxamato single-ion magnets"

Araujo Junior, C. R.; Murad, L. M.; Perrella, R. V.; Oliveira, W. X. C.; Pinheiro, C. B.; Ramos, T. F.; Patricio, P. S. O.; Pedroso, E. F.; Nunes, W. C.; **Ribeiro, P. R. T.*; Muraca, D.*; Fabris, F.*; Knobel, M.***; Sigoli, F. A.; Pereira, C. L. M.

Single-ion magnets (SIMs) are prominent candidates for promoting new technologies in quantum information processing (QIP). Herein, we present two new isostructural oxamato derivatives, namely, {n-Bu4N[Ln(H2edpba)2]}n, Ln = Tb3+ (1) and Gd3+ (2) [H2edpba2- = N,N '-2,2 '-ethylenediphenylenebis(oxamate)], that are thermostable up to similar to 290 degrees C. Single-crystal X-ray diffraction reveals that 1 and 2 are one--dimensional coordination polymers with a ribbon-like structure, and their metal centers are eight-coordinated with a D4d symmetry. Cryomagnetic studies disclose the presence of slow magnetic relaxation (SMR) behavior for 1 and 2. For 1, the Raman effect dominates the SMR at a zero magnetic field, while Raman, Orbach, and reciprocating thermal behavior (RTB) mechanisms arise at higher fields. Conversely, RTB and the bottleneck effect were observed at 2. Solid-state photoluminescent data display a remarkable green luminescence emission, with intense and sharp bands ranging from 480 to 700 nm in the spectra, which are attributed to the 5D4 -> 7FJ (J = 6-0) transitions of terbium(iii) ions. By monitoring the temperature--dependent lifetime of the 5D4 state after the intensity decay of the emission band attributed to the 5D4 -> 7F5 (546 nm) transition, the complex shows a reasonable thermometric performance with a relative sensitivity of 2.77% K-1 at 448 K. 1 behaves as a zero-field SIM and as a photoluminescent thermometer.

INORGANIC CHEMISTRY FRONTIERS, 2025. DOI: 10.1039/d5qi01603g Early Access Date: SEP 2025. **Acesso: https://doi.org/10.1039/D5QI01603G**

[P293-2025] "Reweighting simulated events using machine--learning techniques in the CMS experiment"

Hayrapetyan, A.; Tumasyan, A.; **Chinellato, J. A.*;** et al.
CMS Collaboration

Data analyses in particle physics rely on an accurate simulation of particle collisions and a detailed simulation of detector effects to extract physics knowledge from the recorded data. Event generators together with a geant-based simulation of the detectors are used to produce large samples of simulated events for analysis by the LHC experiments. These simulations come at a high computational cost, where the detector simulation and reconstruction algorithms have the largest CPU demands. This article describes how machine-learning (ML) techniques are used to reweight simulated samples obtained with a given set of parameters to samples with different parameters or samples obtained from entirely different simulation programs. The ML reweighting method avoids the need for simulating the detector response multiple times by incorporating the relevant information in a single sample through event weights. Results are presented for reweighting to model variations and higher--order calculations in simulated top quark pair production at the LHC. This ML-based reweighting is an important element of the future computing model of the CMS experiment and will facilitate precision measurements at the High-Luminosity LHC.

EUROPEAN PHYSICAL JOURNAL C 85[5], 495, 2025. DOI: 10.1140/epjc/s10052-025-14097-x. **Acesso: https://doi.org/10.1140/epjc/s10052-025-14097-x**

[P294-2025] "Search for Fractionally Charged Particles in Proton-Proton Collisions at √s=13 TeV"

Hayrapetyan, A.; Tumasyan, A.; **Chinellato, J. A.***; et al.
CMS Collaboration

A search is presented for fractionally charged particles with charges below 1e, using their small energy loss in the tracking detector as a key variable to observe a signal. The analyzed dataset corresponds to an integrated luminosity of 138 fb(-1) of proton-proton collisions collected at root s = 13 TeV in 2016-2018 at the CERN LHC. This is the first search at the LHC for new particles with a charge between e/3 and 0.9e, including an extension of previous results at a charge of 2e/3. Masses up to 640 GeV and charges as low as e/3 are excluded at 95% confidence level. These are the most stringent limits to date for the considered Drell-Yan-like production mode.

PHYSICAL REVIEW LETTERS 134[13], 131802, 2025. DOI: 10.1103/PhysRevLett.134.131802. **Acesso: https://doi.org/10.1103/PhysRevLett.134.131802**

[P295-2025] "Search for heavy neutral Higgs bosons A and H in the t(t)over-barZ channel in proton-proton collisions at 13 TeV"

Hayrapetyan, A.; Tumasyan, A.; **Chinellato, J. A.***; et al.
CMS Collaboration

A direct search for new heavy neutral Higgs bosons A and H in the t (t) over barZ channel is presented, targeting the process pp -> A -> ZH with H -> t (t) over bar. For the first time, the channel with decays of the Z boson to muons or electrons in association with all-hadronic decays of the t (t) over bar system is targeted. The analysis uses proton-proton collision data collected at the CERN LHC with the CMS experiment at root s = 13 TeV, which correspond to an integrated luminosity of 138 fb(-1). No signal is observed. Upper limits on the product of the cross section and branching fractions are derived for narrow resonances A and H with masses up to 2100 and 2000GeV, respectively, assuming A boson production through gluon fusion. The results are also interpreted within two-Higgs-doublet models, where A and H are CP-odd and CP-even states, respectively, complementing and substantially extending the reach of previous searches.

PHYSICS LETTERS B 866, 139568, 2025. DOI: 10.1016/j.physletb.2025.139568. **Acesso: https://doi.org/10.1016/j.physletb.2025.139568**

[P296-2025] "Search for heavy neutral resonances decaying to tau lepton pairs in proton-proton collisions at √s=13 TeV"

Hayrapetyan, A.; Tumasyan, A.; **Chinellato, J. A.***; et al.
CMS Collaboration

A search for heavy neutral gauge bosons (Z ') decaying into a pair of tau leptons is performed in proton-proton collisions at root s =13 TeV at the CERN LHC. The data were collected with the CMS detector and correspond to an integrated luminosity of 138 fb(-1). The observations are found to be in agreement with the expectation from standard model processes. Limits at 95% confidence level are set on the product of the Z ' production cross section and its branching fraction to tau lepton pairs for a range of Z ' boson masses. For a narrow resonance in the sequential standard model scenario, a Z ' boson with a mass below 3.5 TeV is excluded. This is the most stringent limit to date from this type of search.

PHYSICAL REVIEW D 111[11], 112004, 2025. DOI: 10.1103/PhysRevD.111.112004. **Acesso: https://doi.org/10.1103/PhysRevD.111.112004**

[P297-2025] "Search for high-mass resonances in a final state comprising a gluon and two hadronically decaying W bosons in proton-proton collisions at √s=13 TeV"

Hayrapetyan, A.; Tumasyan, A.; **Chinellato, J. A.*;** et al.
CMS Collaboration

A search for high-mass resonances decaying into a gluon, g, and two W bosons is presented. A Kaluza-Klein gluon, gKK, decaying in cascade via a scalar radion R, g(KK) -> gR -> gWW, is considered.

The final state studied consists of three large-radius jets, two of which contain the products of hadronically decaying W bosons, and the third one the hadronization products of the gluon. The analysis is performed using proton-proton collision data at root s = 13TeV collected by the CMS experiment at the CERN LHC during 2016-2018, corresponding to an integrated luminosity of 138 fb(-1). The masses of the gKK and R candidates are reconstructed as trijet and dijet masses, respectively. These are used for event categorization and signal extraction. No excess of data events above the standard model background expectation is observed. Upper limits are set on the product of the gKK production cross section and its branching fraction via a radion R to gWW. This is the first analysis examining the resonant WW+jet signature and setting limits on the two resonance masses in an extended warped extra-dimensional model.

JOURNAL OF HIGH ENERGY PHYSICS [2], 199, 2025. DOI: 10.1007/JHEP02(2025)199. **Acesso: https://doi.org/10.1007/JHEP02(2025)199**

[P298-2025] "Search for jet quenching with dijets from high--multiplicity pPb collisions at √sNN=8.16 TeV"

Chekhovsky, V.; Hayrapetyan, A.; **Chinellato, J. A.***; et al.
CMS Collaboration

The first measurement of the dijet transverse momentum balance x(j) in proton-lead (pPb) collisions at a nucleon-nucleon center-of-mass energy of root s(NN) = 8.16 TeV is presented. The x(j) observable, defined as the ratio of the subleading over leading jet transverse momentum in a dijet pair, is used to search for jet quenching effects. The data, corresponding to an integrated luminosity of 174.6 nb(-1), were collected with the CMS detector in 2016. The x(j) distributions and their average values are studied as functions of the charged-particle multiplicity of the events and for various dijet rapidity selections. The latter enables probing hard scattering of partons carrying distinct nucleon momentum fractions x in the proton- and lead--going directions. The former, aided by the high-multiplicity triggers, allows probing for potential jet quenching effects in high-multiplicity events (with up to 400 charged particles), for which collective phenomena consistent with quark-gluon plasma (QGP) droplet formation were previously observed. The ratios of x(j) distributions for high- to low-multiplicity events are used to quantify the possible medium effects. These ratios are consistent with simulations of the hard-scattering process that do not include QGP production. These measurements set an upper limit on medium-induced energy loss of the subleading jet of 1.26% of its transverse momentum at the 90% confidence level in high multiplicity pPb events.

JOURNAL OF HIGH ENERGY PHYSICS [7], 118, 2025. DOI: 10.1007/JHEP07(2025)118. **Acesso: https://doi.org/10.1007/JHEP07(2025)118**

[P299-2025] "Search for the Anomalous Events Detected by ANITA Using the Pierre Auger Observatory"

Halim, A. A.; Abreu, P.; **Bonneau Arbeletche, L.*; Chinellato, J. A.*; Dobrigkeit, C.*; Fauth, A. C.*; Machado Payeras, A.*; Reginatto Akim, J. V.*;** et al.
Pierre Auger Collaboration

A dedicated search for upward-going air showers at zenith angles exceeding 110 degrees and energies E > 0.1 EeV has been performed using the Fluorescence Detector of the Pierre Auger Observatory. The search is motivated by two "anomalous" radio pulses observed by the ANITA flights I and III that appear inconsistent with the standard model of particle physics. Using simulations of both regular cosmic-ray showers and upward-going events, a selection procedure has been defined to separate potential upward-going candidate events and the corresponding exposure has been calculated in the energy range [0.1-33] EeV. One event has been found in the search period between January 1, 2004, and December 31, 2018, consistent with an expected background of 0.27 +/- 0.12 events from misreconstructed cosmic-ray showers. This translates to an upper bound on the integral flux of (7.2 +/- 0.2) x 10(-21) cm(-2) sr(-1) y(-1) and (3.6 +/- 0.2) x 10(-20) cm(-2) sr(-1) y(-1) for an E-1 and E-2 spectrum, respectively. An upward-going flux of showers normalized to the ANITA observations is shown to predict over 34 events for an E-3 spectrum and over 8.1 events for a conservative E-3 spectrum, in strong disagreement with the interpretation of the anomalous events as upward-going showers.

PHYSICAL REVIEW LETTERS 134[12], 121003, 2025. DOI: 10.1103/PhysRevLett.134.121003. **Acesso: https://doi.org/10.1103/PhysRevLett.134.121003**

[P300-2025] "Structure and elastic properties of titanium MXenes: Evaluation of COMB3, REAXFF and MEAM force fields"

Thomazini, L. F. V.*; Fonseca, A. F.*

Titanium carbide and nitride MXenes are two-dimensional inorganic materials that exhibit noteworthy physical and chemical properties. These materials are considered for a variety of technological applications, ranging from energy harvesting to optical and biomedical applications. Given the growing interest in titanium MXenes, there is an expanding demand for computational studies to predict physical properties and behaviors under diverse physical conditions. Complex and large-scale systems necessitate computational methodologies that surpass the constraints imposed by ab initio calculations. In this regard, it is imperative to ascertain the reliability of the computational tools employed to simulate and predict the physical properties of titanium MXenes. In this study, the ability of three known classical molecular dynamics (MD) potentials to provide the structural and elastic properties of titanium carbide and nitride MXenes is evaluated. The MD potentials that were the focus of this study include the Charge-Optimized Many-Body (COMB3), the Reactive Force Field (REAXFF) and the Modified Embedded Atom Method (MEAM). These three potentials possess two or more sets of parameters, herein referred to as force fields, capable of simulating Ti-C and Ti-N systems. The MD results for the lattice parameter, thickness and elastic constants of the MXenes are then compared to those from DFT calculations found in the literature. A total of ten force fields were considered; of these, two REAXFF and two MEAM ones were identified as the most adequate to simulate both the structure and elastic properties of titanium MXenes. Additionally, the values for the linear compressibility of MXenes are presented for the first time. Consequently, researchers can utilize the obtained results to design novel MD--based computational studies of titanium MXenes, leveraging the established relative validity of the available force fields.

COMPUTATIONAL MATERIALS SCIENCE 259, 114134, 2025. DOI: 10.1016/j.commatsci.2025.114134. **Acesso: https://doi.org/10.1016/j.commatsci.2025.114134**

[P301-2025] "The role of the reference electrode in EEG recordings: looking from an inverted perspective"

Melo, G. C. de*; Forner-Cordero, A.; **Castellano, G.***

The electroencephalographic signal variability caused by the active reference electrode is a major challenge for classification of motor tasks in Brain-Computer Interfaces. In this work a strategy to deal with the reference is proposed: use the information from all channels to extract more reliable information from the reference, the Inverted Perspective Reference Electrode (IPRE).

In this novel approach the original set of signals is re-referenced to the electrode of interest, in contrast with all other available methods. At total, eight scenarios were analyzed independently: C3 and C4 as reference electrode, alpha and beta frequency bands, and motor imagery and motor execution tasks. Principal Component Analysis (PCA) was used to extract the information from the reference. This information was analyzed by means of the separability between motor tasks. Thirty-six subsets of electrodes were analyzed, including four typical choices of channels for comparison. A dataset with 109 subjects was used. Results showed that the quantity and location of electrodes are determinant to provide class-separable signals at the reference electrode. The IPRE showed greater separability compared to typical channel choices. Therefore, the strategy revealed better outcomes, encouraging further investigation with the inverted perspective to overcome the challenge of the active reference.

BIOMEDICAL PHYSICS & ENGINEERING EXPRESS 11[5], 055048, 2025. DOI: 10.1088/2057-1976/ae093f. **Acesso: https://iopscience.iop.org/article/10.1088/2057-1976/ae093f**

[P302-2025] "Two-dimensional talc as a natural abundant ultra-broadband hyperbolic material"

Feres, F. H.; Maia, F. C. B.; Chen, S.; Mazzotti, V.; **Mayer, R. A.***; Obst, M.; Hatem, O.; Wehmeier, L.; Nörenberg, T.; Queiroz, M. S.; Klopf, J. M.; Kehr, S. C.; Eng, L. M.; Cadore, A. R.; Hillenbrand, R.; Freitas, R. O.; Barcelos, I. D.

We demonstrate that two-dimensional talc, a naturally abundant phyllosilicate mineral, supports hyperbolic phonon-polaritons (HPhPs) across the mid- and far-infrared wavelengths. Using scattering scanning near-field optical microscopy (s-SNOM) and synchrotron infrared nano-spectroscopy (SINS), we reveal tunable HPhP modes in talc flakes with long lifetimes, high confinement, and quality factors of up to 5. We further observe Fabry-P érot cavity modes in tapered flakes, confirmed by simulations and analytical modeling. Compared to synthetic crystals, talc offers an ultra-broadband, low-cost, and sustainable platform for infrared nanophotonics and optoelectronics.

NANOSCALE, 2025. DOI: 10.1039/d5nr02966j Early Access Date: SEP 2025. **Acesso: https://doi.org/10.1039/D5NR02966J**

[P303-2025] "Unlocking efficient charge transport in PSCs: The critical role of oxidizing agents in PEALD NiOx thin films"

Hidrogo-Rico, Mario A.; Mendivil-Palma, I.; Horley, P.; Aguirre-Tostado, F. S.; Quintero-Borbon, F.; Martinez-Guerra, E.; **Guzman, D. G.***; Martinez-Puente, M. A.; **Marques, F. C.***; Martinez-Guerra, E.

This study reports on electronic properties and cationic defects in the thin films of non-stoichiometric nickel oxide (NiOx) synthesized with plasma-enhanced atomic layer deposition (PEALD). Starting from nickel acetylacetonate [Ni(acac)2] as a metal-organic precursor, we employed water (P-W), ozone (P-Oz), and oxygen plasma (P-Ox) as oxidizing agents for direct plasma-enhanced ALD (DPALD) to evaluate their impact on the electronic structure of NiOx. The primary objective is to identify the most suitable oxidizing agent for producing NiOx films with optimal performance for hole transport layers (HTLs) in optoelectronic devices. Angle-resolved X-ray photoelectron spectroscopy (AR-XPS) confirmed the non-stoichiometric nature of our films. Measurements made at the 45 degrees take-off angle revealed significant variations in the Ni2+/Ni3+ ratio depending on the oxidizing agent chosen, increasing from 0.80 (P-W) to 0.89 (P-Ox). This trend indicates improved defect formation control, permitting to achieve valence band shift of 0.98 eV for P-Ox sample relative to EV of MAPbI3. Additionally, reflection electron energy loss spectroscopy (REELS) revealed band gap narrowing from 3.53 eV (P-W) to 3.38 eV (P-Ox), suggesting enhancement of electronic properties. Band alignment analysis based on XPS and REELS data demonstrates that NiOx films synthesized with oxygen plasma exhibit favorable band alignment with MAPbI3 perovskite. Moreover, contact angle measurements reveal that subtle changes in defect chemistry affect the wettability of NiOx surfaces with respect to perovskite precursor solutions. Put together, these findings identify oxygen plasma-assisted synthesis as the most promising strategy for fabricating NiOx-based HTLs with superior electronic properties and advantageous interface characteristics, which are promising for the next-generation optoelectronic devices. This work emphasizes the importance of PEALD oxidazing agent choice for achieving a precise tailoring of NiOx electronic structure and enhancing the resulting device performance.

MATERIALS SCIENCE IN SEMICONDUCTOR PROCESSING 200, 109969, 2025. DOI: 10.1016/j.mssp.2025.109969. **Acesso: https://doi.org/10.1016/j.mssp.2025.109969**

Correções

[Co003-2025] "Combination of the TD-DFT and the pixel counting method for determining electron capture cross sections for protons impacting on organic molecules (vol 79, 111, 2025)"

Oliveira, L. A. de*; Faria, J. C. de*; Bernal, M. A.*

EUROPEAN PHYSICAL JOURNAL D 79[9], 111, 2025. DOI: 10.1140/epjd/s10053-025-01054-2. **Acesso: https://doi.org/10.1140/epjd/s10053-025-01054-2**

[Co004-2025] "fNIRS reproducibility varies with data quality, analysis pipelines, and researcher experience (vol 8, 1149, 2025)"

Yücel, M. A.; Luke, R.; **Mesquita, R. C.*; Martins, G. G.***; et al.

COMMUNICATIONS BIOLOGY 8[1], 1256, 2025. DOI: 10.1038/s42003-025-08714-4. **Acesso: https://doi.org/10.1038/s42003-025-08714-4**

[Co005-2025] "Nanophotonics of mid-infrared plasmon-polaritons at interfaces between metals and two-dimensional crystals (vol 17, 13229-13237, 2025)"

Feres, F. H.; Barcelos, I. D.; Bahamon, D. A.; Levandoski, J. E.; Mancini, A.; Santos, T. M. dos; **Mayer, R. A.*;** Camargo, D. H. S.; Bufon, C. C. B.; Cernescu, A.; Maier, S. A.; Freitas, R. D. de O.; Maia, F. C. B.

NANOSCALE 17[34], p. 19966-19966, 2025. DOI: 10.1039/d5nr90162f. **Acesso: https://doi.org/10.1039/D5NR90162F**

***Autores da comunidade IFGW**
Fonte: Web of Science on-line (WOS)

Cartas

[Ca001-2025] "Determination of the strong coupling and its running from measurements of inclusive jet production"

Chekhovsky, V.; Hayrapetyan, A.; **Chinellato, J. A.*;** et al.
CMS Collaboration

The value of the strong coupling aS is determined in a comprehensive analysis at next-to-next-to-leading order accuracy in quantum chromodynamics. The analysis uses double-differential cross section measurements from the CMS Collaboration at the CERN LHC of inclusive jet production in proton-proton collisions at centre-ofmass energies of 2.76, 7, 8, and 13TeV, combined with inclusive deep-inelastic data from HERA. The value aS(aZ)=0.1176 +0.0014 −0.0016 is obtained at the scale of the Z boson mass. By using the measurements in different intervals of jet transverse momentum, the running of aS is probed for energies between 100 and 1600GeV.

PHYSICS LETTERS B 868, 139651, 2025. DOI: 10.1016/j.physletb.2025.139651. **Acesso:** https://doi.org/10.1016/j.physletb.2025.139651

[Ca002-2025] "Measurement of the Drell-Yan forward-backward asymmetry and of the evffective leptonic weak mixing angle in proton-proton collisions at √s=13TeV"

Hayrapetyan, A.; Tumasyan, A.; **Chinellato, J. A.*;** et al.
CMS Collaboration

The forward-backward asymmetry in Drell-Yan production and the effective leptonic electroweak mixing angle are measured in proton-proton collisions at root s= 13 TeV, collected by the CMS experiment and corresponding to an integrated luminosity of 138 fb(-1). The measurement uses both dimuon and dielectron events, and is performed as a function of the dilepton mass and rapidity. The unfolded angular coefficient A(4) is also extracted, as a function of the dilepton mass and rapidity. Using the CT18Z set of parton distribution functions, we obtain sin(2) theta(l)(eff)= 0.23152 +/- 0.00031, where the uncertainty includes the experimental and theoretical contributions. The measured value agrees with the standard model fit result to global experimental data. This is the most precise sin(2) theta(l)(eff) measurement at a hadron collider, with a precision comparable to the results obtained at LEP and SLD.

PHYSICS LETTERS B 866, 139526, 2025. DOI: 10.1016/j.physletb.2025.139526. **Acesso:** https://doi.org/10.1016/j.physletb.2025.139526

Conjunto de Dados

[D001-2025] "Supplementary Materials_ACS Omega_CTiO2"

Destefani Paquini, L.*; Togneri Marconsini, L.; Sanches De Lima, B.; Profeti, L.; Ribeiro, J.; Profeti, D.

Datasets refered to supplementary materials from article intitled "Synthesis, Characterization, and Application of an Ecofriendly C/TiO2 Composite to Efficiently Remove Reactive Black 5 (RB-5) Textile Dye from Aqueous Solutions" Copyright: Creative Commons Attribution 4.0 International.

Mendeley Data, V1, 2025. DOI: 10.17632/hd7nx94mr4.1. **Acesso:** https://data.mendeley.com/datasets/hd7nx94mr4/1

***Autores da comunidade IFGW**
Fonte: Web of Science on-line (WOS)

Defesas de Dissertações do IFGW

[D016-2025] "O vértice de três-glúons na presença de quarks dinâmicos"
Aluno: Laís Almeida Wendland
Orientador: Profa. Dra. Arlene Cristina Aguilar
Data: 02/10/2025

[D017-2025] "Violação de Simetria CP em decaimentos charmosos: nova Física ou efeitos não-perturbativos?"
Aluno: Bruna Heluá Cabalin Tibúrcio
Orientador: Profa. Dra. Patrícia Camargo Magalhães
Data: 24/10/2025

[D018-2025] "Avaliação de redes funcionais de dados de EEG de indivíduos sob efeito de Ayahuasca"
Aluno: Marcelo Fernando Tisoc Mora
Orientador: Profa. Dra. Gabriela Castellano
Data: 24/10/2025

Defesas de Teses do IFGW

[T012-2025] "Estudo da performance do sistema de fotodetecção do ProtoDUNE"
Aluno: Renan de Aguiar
Orientador: Prof. Dr. Ettore Segreto
Data: 17/10/2025

[T013-2025] "Conversão de Sabor em Neutrinos de Supernovas"
Aluno: Pedro Dedin Neto
Orientador: Prof. Dr. Ernesto Kemp
Data: 23/10/2025

[T014-2025] "Sincronização de motifs para caracterizar epilepsia"
Aluno: Leonardo Rodrigues da Costa
Orientador: Profa. Dra. Gabriela Castellano
Data: 31/10/2025

[T015-2025] "Uso de modelos biofísicos para estimar relatividade biológica de isótopos usados em Targeted Radionuclide Therapy"
Aluno: William Toshio Watanabe Jugue
Orientador: Prof. Dr. Mario Antonio Bernal Rodriguez
Data: 05/11/2025

[T016-2025] "Propriedades não perturbativas de vértices da QCD e sua conexão com a geração dinâmica de massa"
Aluno: Bianca Maria Silveira de Oliveira
Orientador: Profa. Dra. Arlene Cristina Aguilar
Data: 17/11/2025

[T017-2025] “Quantização de Modos Instáveis em Espaços Não-Globalmente Hiperbólicos”
Aluno: Bruno Santos Felipe
Orientador: Prof. Dr. João Paulo Pitelli Manoel
Data: 24/11/2025

[T018-2025] “Uma perspectiva físico-química em Termo-cronologia por Traços de Fissão”
Aluno: Matheus Rufino
Orientador: Prof. Dr. Sandro Guedes de Oliveira
Data: 01/12/2025

Fonte: Portal IFGW/Eventos
Disponível em: https://portal.ifi.unicamp.br/a-instituicao/eventos/month.calendar/2025/08/22/-

Novidade:
Acesse os trabalhos pelos links!!

Abstracta

Instituto de Física Gleb Wataghin
Diretor: Prof. Dr. Marcos Cesar de Oliveira
Universidade Estadual de Campinas - UNICAMP
Cidade Universitária Zeferino Vaz
13083-859 - Campinas - SP - Brasil
e-mail: secdir@ifi.unicamp.br
Fone: +55 19 3521-5300

Publicação

Biblioteca do Instituto de Física Gleb Wataghin
http://portal.ifi.unicamp.br/biblioteca
Instagram: @bif.unicamp

Diretora Técnica: Sandra Maria Carlos Cartaxo
Coordenadora da Comissão de Biblioteca: Profa. Dra. Arlene Cristina Aguilar

Elaboração e editoração:
Maria Graciele Trevisan (Bibliotecária)
Contato: infobif@ifi.unicamp.br